



## Review article

## Towards multiscale X-ray tomographic imaging in membrane science — A perspective

Gregor Rudolph-Schöpping<sup>a,b,\*</sup>, Emanuel Larsson<sup>b,c,d,e</sup>, Torben Nilsson Pingel<sup>f</sup>,  
Manuel Guizar-Sicairos<sup>g,h</sup>, Pablo Villanueva-Perez<sup>e,i</sup>, Stephen Hall<sup>b,c</sup>, Frank Lipnizki<sup>a,b</sup>

<sup>a</sup> Department of Chemical Engineering, Lund University, 22100 Lund, Sweden

<sup>b</sup> LINXS - Institute of Advanced Neutron and X-ray Science, Lund, Sweden

<sup>c</sup> Division of Solid Mechanics, Department of Construction Sciences, Lund University, Lund, Sweden

<sup>d</sup> LUNARC Centre for Scientific and Technical Computing, Lund University, Lund, Sweden

<sup>e</sup> MAX IV Laboratory, Lund University, Lund, Sweden

<sup>f</sup> RISE Research Institutes of Sweden, Bioeconomy and Health - Agriculture and Food, Gothenburg, Sweden

<sup>g</sup> Paul Scherrer Institute, Villigen PSI, Switzerland

<sup>h</sup> Institute of Physics, École Polytechnique Fédérale de Lausanne (EPFL), Lausanne, Switzerland

<sup>i</sup> Division of Synchrotron Radiation Research and NanoLund, Department of Physics, Lund University, Lund, Sweden

## ARTICLE INFO

## Keywords:

Membrane characterisation

Microtomography

Holotomography

Nanotomography

Ptychotomography

## ABSTRACT

Tomographic X-ray imaging techniques offer novel opportunities for studying membranes and membrane processes in 3D on a spatial resolution not seen before. Traditional 2D imaging techniques used to characterise membranes have limitations that can be overcome by tomographic X-ray imaging. Tomographic X-ray imaging can provide information in 2D/3D or 4D (3D plus time) on membranes, membrane modules, and membrane processes on a scale ranging from micro- to nanometre. They offer the possibility to uncover many fundamental issues related to membrane science, including the detection and monitoring of macroscopic biofilm formation, scaling, and cake build-up. High-resolution nanotomographic X-ray imaging enables even microscopic characterisations such as pore size distribution or pore network analysis. This Perspective paper introduces the tomographic X-ray imaging techniques with the most potential for membrane science: microtomography, nanotomography, holotomography, and ptychotomography, and presents their applications in the literature regarding the field of membrane science. Based on these findings and our experiences opportunities, challenges, and limitations of tomographic X-ray imaging techniques are discussed. It is concluded that in the near future tomographic X-ray imaging techniques will become increasingly common analytical techniques for membrane manufacturers, scientists, and users.

## 1. Introduction

Membrane processes are highly selective, electrifiable, and low-energy demanding unit operations and are therefore already employed in a wide range of industries. In 2021, the global membrane market exceeded 24.7 billion Euro and is expected to grow by a rate of 12.2% annually until 2030 [1]. A prerequisite for the expected growth is a continued development in the field of membrane science. Key fundamental physical properties that ensure high separation efficiency and flux are determined by the manufacturing process of the membrane and membrane module, as well as the conditions during operation. The development of new commercial membranes and their applications are restricted by four key hurdles: (1) material conversion into a novel membrane; (2) membrane module assembly; (3) module integration

into a membrane process; (4) membrane process incorporation into a production process [2]. Overcoming these hurdles necessitates considering and understanding a combination of various factors and a comprehensive characterisation of the membrane after each of the hurdle, before, during (*in situ/operando*), and after (*post-mortem*) usage. The characterisation becomes challenging when it is to be performed *in situ/operando* and dynamic properties during filtration are to be investigated too.

Most membranes possess an asymmetric structure, often consisting of several distinct layers, with some of them being dense while others being porous. The structural and mechanical characterisation of the bulk and surface properties of the membranes requires a wide range of techniques spanning many orders of magnitude in spatial resolution,

\* Corresponding author at: Department of Chemical Engineering, Lund University, 22100 Lund, Sweden.

E-mail address: [Gregor.rudolph-schopping@chemeng.lth.se](mailto:Gregor.rudolph-schopping@chemeng.lth.se) (G. Rudolph-Schöpping).

<https://doi.org/10.1016/j.memsci.2023.122245>

Received 15 June 2023; Received in revised form 23 October 2023; Accepted 2 November 2023

Available online 8 November 2023

0376-7388/© 2023 The Author(s). Published by Elsevier B.V. This is an open access article under the CC BY license (<http://creativecommons.org/licenses/by/4.0/>).

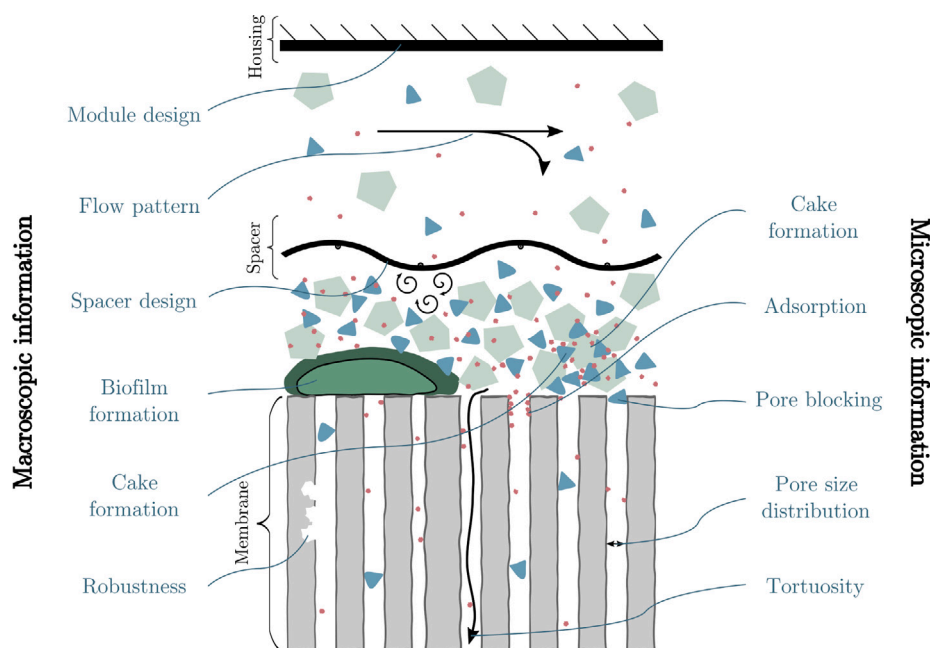


Fig. 1. Schematic overview of macroscopic and microscopic phenomena related to pressure-driven membrane processes. (For interpretation of the references to colour in this figure legend, the reader is referred to the web version of this article.)

starting at the atomic scale and ranging to metres. Macroscopic phenomena require resolutions in the range of millimetre to micrometre, while microscopic phenomena require resolutions in the nanometre range. Common details of interest on the example of pressure-driven membrane processes are illustrated in Fig. 1.

According to Khulbe and Matsuura [3] “an ideal characterisation method should be non-destructive, accurate, repeatable, and fast”, while maximising data output. A technique fulfilling these requirements and already used in many fields is tomographic X-ray imaging. One of the crucial advantages of X-rays over visible photons or electrons is their larger penetration length. Tomographic X-ray imaging is a set of non-destructive imaging techniques that can be used to produce three-dimensional images of objects on a wide spatial range. This is very promising for membrane research as from many scientific questions in the field, information in two-dimensions (2D) is not sufficient, while data in three-dimensions (3D) provides the needed information.

Tomographic imaging techniques that can achieve resolutions of 1  $\mu\text{m}$  on samples of mm or even cm scale, such as microtomography, be used to improve the housing, the spacer or to characterise a cake layer or a gel layer (see 1). Fast techniques such as synchrotron-radiation-based techniques can be used for in situ studies. Furthermore, techniques that enable high resolution imaging such as nanotomography, holotomography, and ptychotomography, can be used to study phenomena on the nanoscale such as scaling, membrane fouling based on adsorption or pore blocking, or for the characterisation of the inner structure of the membrane in terms of e.g., pore size distribution, tortuosity, or chemical robustness.

Until now, tomographic X-ray imaging techniques, such as full-field X-ray microtomography, X-ray nanotomography, and scanning X-ray nanotomography techniques (i.e. ptychotomography) have been used only to a limited extent to study synthetic membranes and membrane process phenomena. So far, a pioneering and comprehensive book chapter on the use of tomographic X-ray imaging in membrane science has been published by Remigy [4] in 2009 and five years later, the use of synchrotron radiation micro- and nanotomography in membrane science has been described as part of a review on recent advances in the field of membrane morphology by Tung et al. [5]. Furthermore, a focused review on the characterisation of anion-exchange membranes for water electrolyzers and fuel cells has been published by Yang et al. [6]

including a chapter on X-ray computed tomography. In contrast to the previous work, the present Perspective paper provides an updated summary of the limitations of conventional analytical techniques for the structural and mechanical characterisation of membranes; a brief theoretical background on four relevant tomographic X-ray imaging techniques: (i) microtomography ( $\mu\text{CT}$ ), (ii) nanotomography (nCT), (iii) holotomography, and (iv) ptychotomography (PXCT), including advantages and disadvantages; a summary of studies related to membrane science that have applied these techniques; and a discussion on opportunities, challenges, and limitations that these techniques hold with regards to membrane science.

## 2. Limitations of conventional methods to characterise membranes

Structural and mechanical properties of membranes have been characterised with various indirect and direct techniques before [7], but these conventional techniques have limitations that can be overcome by tomographic X-ray imaging. This section provides a brief overview on indirect and direct characterisation techniques, excluding tomographic X-ray imaging, and their limitations for the characterisation of structural and mechanical properties of membranes.

Indirect invasive methods for the characterisation of mechanical properties of membranes such as the pore size distribution or porosity include bubble point pressure analysis, gas–liquid displacement porometry, [8,9], liquid–liquid displacement porometry [10], mercury porosimetry [11], gas adsorption and desorption by physisorption analysis [12], or the relatively novel method of membrane impedance porometry [13]. In contrast to tomographic X-ray imaging, these techniques can only determine the largest pore entrance and not the actual inner diameter of a pore channel. Isolated pores not connected to any surface cannot be detected. Moreover, for asymmetric membranes, it remains a challenge to distinguish the porous support layer from the dense active layer. This can be of interest for quality tests of new membranes or when investigating membrane fouling and cleaning. Furthermore, for some of these methods, high pressures need to be applied or the sample needs to be dried extensively and cut into smaller pieces for the analysis, all of which affect the sample structure. For tomographic X-ray imaging, this is not a general prerequisite.

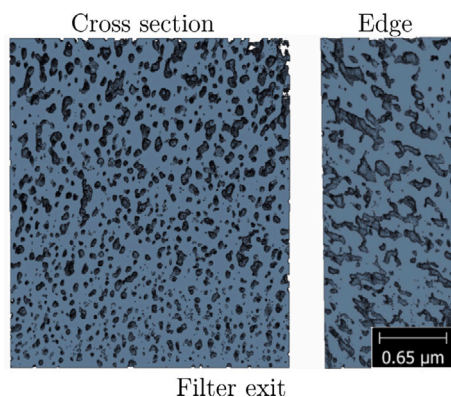


Fig. 2. 3D reconstruction of a membrane obtained from serial sectioning using cryogenic FIB-SEM. The grey structure depicts the polymer region.

Source: Adapted from [15].

© 2021 with permission of Elsevier B.V.

Common visual techniques for direct invasive characterisation are based on optical microscopy, electron microscopy, and scanning probe microscopy. These techniques can be applied to observe the surface morphology of a membrane and to gather information on the surface porosity. With 2D microscopy techniques, such as the electron microscopic techniques scanning electron microscopy (SEM) or transmission electron microscopy (TEM), spatial resolutions well beyond the possibilities of tomographic X-ray imaging techniques can be obtained [14].

For SEM, the membrane typically needs to be dry and sputter-coated (commonly for polymeric membranes) with a thin metal layer to reduce the effect of charging. Besides other effects, this sample preparation technique alters the pore size and pore distribution of the sample. An exception is the usage of environmental SEM, which allows microscopy imaging in wet conditions though at a slightly lower resolution than the common field-emission SEM. Focused-ion beam (FIB) abrasion in combination with SEM (FIB-SEM), also known as serial sectioning, makes it possible to extract information on the 3D structure of a sample [15] (Fig. 2), but the method is very time consuming and only small volumes of the sample can be probed, making it difficult to judge if the results are representative. Another disadvantage is that the membrane structure might be damaged during abrasion, resulting in artefacts in the 3D model. A way to avoid beam-induced specimen damage while still conducting serial sectioning is by combining SEM with a microtome [16] (Fig. 3). The limitation of this method is that it is even more time-consuming than FIB-SEM. Moreover, microtoming can cause more mechanical damage and artefacts to the membrane sample than compared to abrasion with an ion beam. High resolution tomographic X-ray imaging can also require tedious sample preparation but lower resolutions can be reached rather easily and even without any sample preparation.

With TEM, very high spatial resolutions can be reached. In addition, the technique can provide information in 3D, with so called TEM tomography [17], as well as crystallographic (cryo-electron microscopy), and chemical information, but sample preparation is tedious. The sample needs to be embedded in a resin and microtomed into very thin slices. Imaging of larger volumes in 3D (at least several micrometres in each direction), usually required for membranes to get representative results, is not possible with TEM tomography but easily achievable for low resolution tomographic X-ray imaging.

Scanning probe techniques such as atomic force microscopy (AFM) allows the study of the topology of a sample and also the surface porosity [18], but underlying layers are not accessible with this technique. All microscopic techniques have in common that it is difficult to analyse samples that are three dimensional (curved/bent) such as tubular, hollow fibre, spiral-wound or 3D printed membranes. Furthermore, in contrast to tomographic X-ray imaging, *operando* investigations in 4D

(3D + time), where the sample is investigated over a certain operation time or in a changing sample environment, are very challenging with these direct invasive characterisation techniques.

A technique that allows 3D and even 4D analysis and which is related to tomographic X-ray imaging is optical coherence tomography (OCT). OCT is an up-coming technique that has already been used several times for membrane related research, e.g. [19–21] (Figure [20]). It provides 3D data of a sample of any shape, but at a much lower spatial resolution and lower penetration depth than what X-ray-based imaging techniques can provide (see Fig. 4).

As shown, structural and mechanical properties of membranes can be characterised with various techniques. Therefore, tomographic X-ray imaging techniques do not provide entirely unique information. However, in comparison to the more conventional techniques, tomographic X-ray imaging techniques provide novel insight in 3D or even 4D on membranes, membrane modules, and membrane processes with just one technique and on a high spatial and temporal scale not seen before.

### 3. Techniques for X-ray computed tomography of membranes in the micro- and nano-scales

In tomographic X-ray imaging, projection images are acquired over 180 or 360 °, while the sample rotates with respect to the X-ray beam propagation direction. The projection images are then used to reconstruct a 3D volume of the sample, where each voxel is represented by a grey scale value of the linear attenuation coefficient ( $\text{cm}^{-1}$ ) of the sample itself. A voxel, or a volumetric pixel, represents a cube with an edge length of the voxel size and is located on the three-dimensional grid of the sample volume. The best half-pitch resolution achievable by any technique is equal to the voxel size. However, it should be noted that not all instruments and not all measurements will achieve voxel-size resolution. The actual resolution of the measurement has to be taken into account carefully when segmenting and making conclusions of the 3D volume.

The X-ray beam can come from a lab-based X-ray source or from a synchrotron light source. In general, synchrotron X-ray sources offer a higher throughput and reach higher resolutions much faster than lab-based sources as the latter are limited in the available photon flux and brilliance. Moreover, synchrotron light sources offer more flexibility and can have monochromatic X-rays, while lab-based X-ray sources have a fixed spectra of energy of the X-rays to be used. The photon flux of an X-ray beam describes the amount of photons per second. The brilliance of an X-ray beam is a measure of the intensity and directionality and is defined as photon flux per unit source emittance.

Closely related and a physically measurable quantity of brilliance is coherence. This term describes the degree to which the phase of a wave is correlated between any two spatial points. Thus, for a coherent X-ray beam, the electromagnetic waves are synchronised in phase and wavelength. Coherent X-ray beams provide the opportunity to use coherent lensless imaging techniques that can overcome the difficulties of fabricating high-resolution X-ray optics and provide a resolution ultimately limited by the wavelength of the X-rays [22]. Examples of coherent X-ray imaging techniques are coherent diffractive imaging, holotomography, and PXCT.

In this perspective paper, we grouped tomographic X-ray imaging techniques according to their spatial resolution. For  $\mu$ CT, a resolution between 0.5 and 0.7  $\mu\text{m}$  can usually be reached and either a lab-based X-ray source or a synchrotron light source can be used. Nanotomographic X-ray imaging techniques reach a higher spatial resolution and include techniques reaching resolutions in the lower nanometre range. Currently, nanotomographic X-ray imaging can be only done with synchrotron light sources. In the context of this paper, the techniques holotomography, full-field nCT, and PXCT are presented as nanotomographic X-ray imaging techniques.

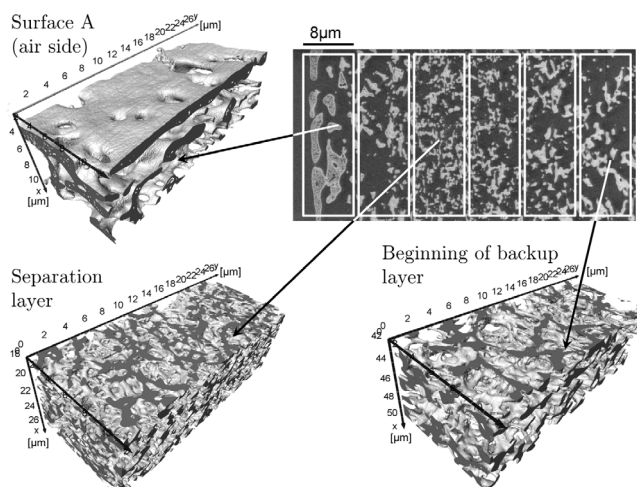


**Fig. 3.** Schematic of the partitioning of a part of a membrane by serial section using microtoming and SEM and corresponding 3D reconstructions. Source: Adapted from [16].

© 2011 with permission of Elsevier B.V.

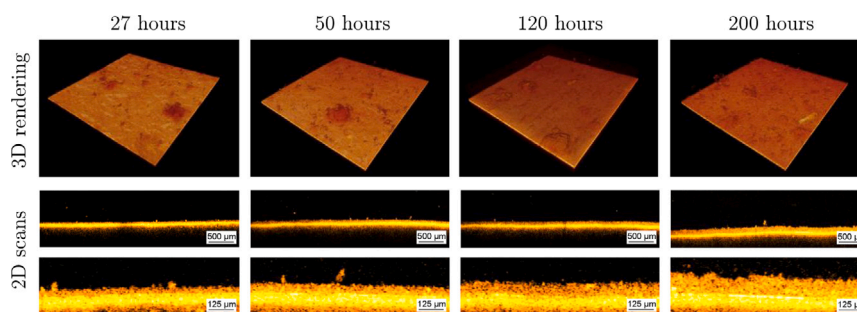


**Fig. 4.** Visualisation of 2D and 3D OCT scans of a cake layer formed on a flat-sheet an membrane bioreactor over the time.

Source: Adapted from [20].

© 2019 with permission of Elsevier B.V.

### 3.1. Microtomography in membrane science

Most of the tomographic X-ray imaging studies related to membrane science and presented in the literature review part of subsequent sections of this work have been conducted with  $\mu$ CT. Two-thirds of the reported  $\mu$ CT experiments were conducted with lab-based instruments, while around one third was conducted at a synchrotron light source. Therefore, the research on  $\mu$ CT presented in this section is separated in the subsections ‘Lab-based X-ray microtomography’ and ‘Synchrotron radiation X-ray microtomography’.

For  $\mu$ CT a nominally flat X-ray illumination is incident on the sample and a pixelated detector downstream detects the attenuated X-rays passing through the sample, from which a transmission projection image can be calculated following Lambert–Beer’s law. These projection images are then digitally reconstructed into tomographic slices. Projection images can be formed by numerous contrast mechanisms based on the different interaction between the X-rays and the object’s cross section. The first and most widespread imaging X-ray contrast is based on absorption. Absorption contrast imaging makes use of the inhomogeneous passage of X-rays through a sample’s distribution of electron density, resulting in varied levels of transmission.

Another contrast used for imaging is phase-contrast. If the sample-to-detector distance is increased, as for  $\mu$ CT, and if the beam has a certain degree of coherence, then propagation effects will appear on the images. In particular, phase differences in the sample will create propagation fringes around edges. These edge effects can be leveraged and thereby a phase-retrieved image can be obtained [14]. When using phase contrast imaging, the measured intensity, with the fringes, can be

processed by a single step so-called ‘phase retrieval’ algorithm such as e.g. Paganin method [23]. With phase retrieval, it is possible to recover the phase from the absorption, to improve the reconstruction, and to deconvolve the propagation fringes [24].

#### 3.1.1. Lab-based X-ray microtomography

The first work using  $\mu$ CT in the field of membrane science was done in the year 2000 by Frank et al. [25] with a clinical X-ray CT scanner. The resolution was several tens of micrometres but the exact value was not stated. The aim of the study was to measure salt concentration fields within a haemodialysis module. It was possible to reveal the distribution of the dialysate flow around hollow fibre dialyser membranes made of cellulose diacetate. A sodium chloride (NaCl) solution was used to create sufficient contrast of the liquid flow in the sample. While this approach provided insights on the variation of salt concentrations through the module, a structural assessment of the membranes was not possible. Module design for improving the filtration performance is still a relevant topic. In an unpublished study, we used  $\mu$ CT to make the distribution of a cake layer in a spiral wound module visible. A commercial UF spiral-wound membrane made from polysulfone (GR61PP 2517/48, Alfa Laval, Nakskov, Denmark) with a molecular weight cut-off (MWCO) of 10 kDa was used to concentrate a calcium carbonate ( $\text{CaCO}_3$ ) suspension (OmyaCarb15-GU Omya AB, Malmö, Sweden, average particle diameter of 15  $\mu\text{m}$ ) at ambient temperature in cross-flow mode. The module was subsequently cleaned with the acidic cleaning agent Ultrasil 78 (Ecolab, Monheim, Germany). After each treatment, lab-based  $\mu$ CT imaging was conducted with an EasyTom150 (RX Solutions, Chavanod, France) at the 4D Imaging Lab

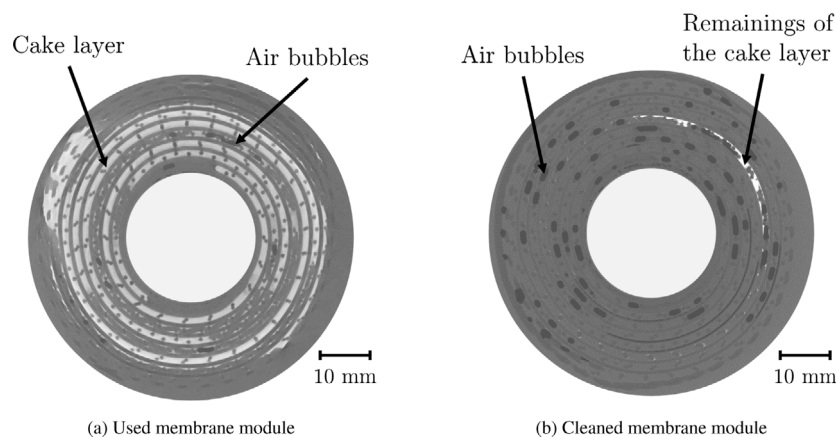


Fig. 5. Tomographic slice of a lab-based X-ray microtomography scan of a commercial spiral wound UF membrane module used for the filtration of  $\text{CaCO}_3$  and the very same membrane after cleaning with an acidic cleaning agent.

at Lund University. Images were acquired over the entire membrane with 8 stacked scans taking about 1 h in total for the full volume. The source setting was 60 keV, the voxel size in the reconstructed 3D images was 50  $\mu\text{m}$ . Tomographic slices showed that the cake was unevenly distributed along the spiral structure of the membrane and the length of the module, Fig. 5. This observation can be used to understand why a cake layer is building up where it is and why it remains present at certain spots after cleaning.

Also the module assembly of ion-exchange membrane fuel cells can be investigated with lab-based  $\mu\text{CT}$ . In a study by Liang et al. [26], the connection between the membrane and the electrode assemblies was imaged to determine the internal stability of this interface during durability tests. Different layers connecting the membrane and the electrode assemblies were tested. It was found that only the presented novel 3D-zipped interface prevented the formation of cracks or crevices.

Furthermore, lab-based  $\mu\text{CT}$  allows to characterise the porous macro-structure of membranes. Viguié et al. [27] used the technique to study hollow fibre membranes spun from polyvinylidene fluoride with N-Methyl-2-pyrrolidone as a solvent and water as a coagulant. Before coagulation, the fibres passed through an air gap zone. They had an outer diameter of 1.2 mm, a outer skin layer thickness of 0.1 mm, and an inner diameter of 0.3 mm. Spinning conditions were varied. The weight percentage of N-Methyl-2-pyrrolidone ranged from 0%(w/w) to 30%(w/w) and the air gap length ranged from 1 cm to 50 cm. A nanofocus  $\mu\text{CT}$  system (Phoenix Nanotom S, Waygate Technologies, Hürth, Germany) was used reaching a voxel size of 1  $\mu\text{m}$ . The fibre length was 5 mm. It was possible to characterise the shape and spatial distribution of macro-voids in the outer and inner layers of the fibres as a function of the varied spinning process conditions. It was found that solvent addition into the bore led to an increase in the width of the macro-voids. Furthermore, the authors could determine a critical residence time in air leading to significantly more macro-voids. In addition, the size of macro-voids close to the inner layer of the fibre increased with residence time. Another early work was done by Vladislavjević et al. [28] that characterised the structure of Shirasu porous glass membranes with lab-based  $\mu\text{CT}$ . The sample height was 2.2 mm and a resolution of 3 to 4  $\mu\text{m}$  was reached. It was possible to characterise the membrane pores (pore size roughly in the range of 9–24  $\mu\text{m}$ ) and to confirm the isotropic property of the membrane. Recently, Bridge et al. [29] investigated macro-voids in nonsolvent-induced phase separation membranes. In their study, segmented cross-sectional images acquired with scanning electron microscopy (SEM) were compared with imaging by  $\mu\text{CT}$ . It was found that the proposed SEM sampling approach was accurate for quantifying macro-porosity in asymmetric membranes prepared by non-solvent-induced phase separation. The macro-porosity determined by SEM was within  $\pm 6\%$  of the value determined with  $\mu\text{CT}$ . However, the loss of 3D

information on macro-void size, shape, and count with the SEM-based approach was highlighted by the authors in their conclusions.

In general, effective image processing allows for 3D quantification and visualisation that clearly demonstrates the possibilities of  $\mu\text{CT}$  for characterising membranes. In Fig. 6(a) (unpublished work by the authors) a 3D rendering of a grey-level threshold polymeric UF membrane (UFX5-pHt, Alfa Laval, Naaskov, Denmark) is presented. The data was acquired using an Xradia Versa 520 (Zeiss, Oberkochen, Germany) at the 4D Imaging Lab at Lund University at 60 keV and a voxel size of 1  $\mu\text{m}$  in the reconstructed 3D images. The images clearly show the pore structure of the support layer of the membrane and even the finger structure of the active layer. According to the manufacturer, the membrane had a MWCO of 5 kDa. A video of the 3D rendered sample can be found in the online version of this paper. With further image processing, individual macro-pores in the support layer can be identified (Fig. 6(b)) and the connection paths highlighted (Fig. 6(c)). This could later be used to determine the pore size distribution, porosity, and tortuosity of the membrane as done for example by Maier et al. [30] for polymer electrolyte membrane water electrolyser liquid-gas diffusion layers. With image processing of lab-based  $\mu\text{CT}$  data, they were able to calculate the porosity and to create pore network models of several liquid-gas diffusion layers. This pore network was then used to determine the pore size distribution and tortuosity of the samples.

Overall, the latest advancement of lab-based  $\mu\text{CT}$  makes it possible to quickly investigate membrane samples at high spatial resolutions. In Fig. 7 (unpublished work by the authors) a tomographic slice of a polyvinylidene difluoride hollow fibre membrane acquired using the Xradia Versa 520 (Zeiss, Oberkochen, Germany) at the 4D Imaging Lab at Lund University at 80 keV is shown and the high quality of lab-based  $\mu\text{CT}$  instruments is clearly visible making the evaluation of the state of a membrane very fast and easy.

Tomographic X-ray imaging also makes it possible to study structural changes of ion-exchange membranes induced by swelling [31]. Svoboda et al. used a heterogeneous cation-exchange membrane made of polyethylene as a binder and polyester fibres for reinforcement. The membranes were soaked in various potassium chloride (KCl) solutions with concentrations from 1 mM to 1 M to cause membrane swelling. The water in the aqueous KCl solutions caused a high absorption of the X-rays, therefore, the authors developed a cell that allowed them to perform  $\mu\text{CT}$  scans in saturated water vapour while avoiding any volumetric changes of the membrane due to water evaporation. The sample size was  $1 \times 1 \text{ mm}^2$  and a resolution of 2.1  $\mu\text{m}$  was reached. It was found that dry pristine membranes contained ion-exchange resin particles with large size variation randomly distributed in the polyethylene binder. In addition, a great number of macro-voids were uncovered. Swelling in the KCl solution caused significant structural changes to the volume of the membrane and the ion-exchange resin particles. The

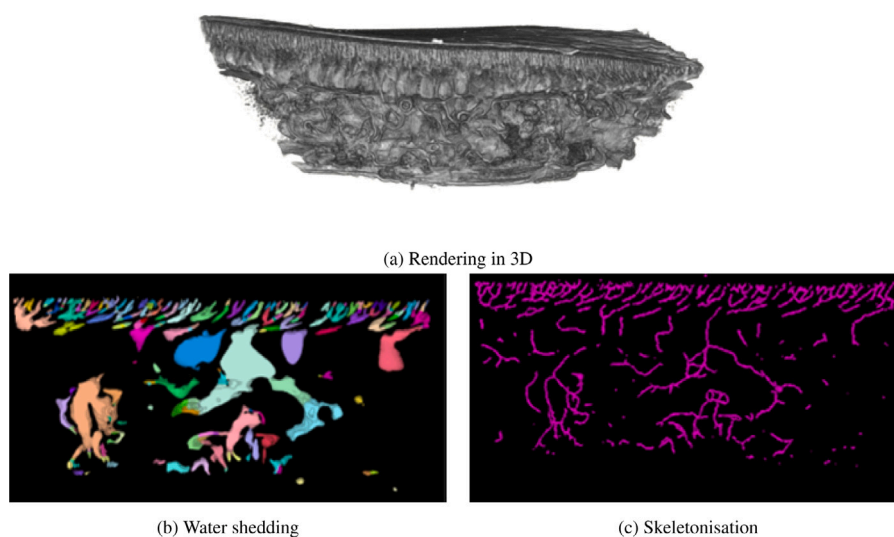


**Fig. 6.** 3D rendering based on threshold-based segmented images of a fouled UF (a) and image processed tomographic slices of the membrane highlighting the pores separated by water shedding (b) and the connection path identified by skeletonisation (c).

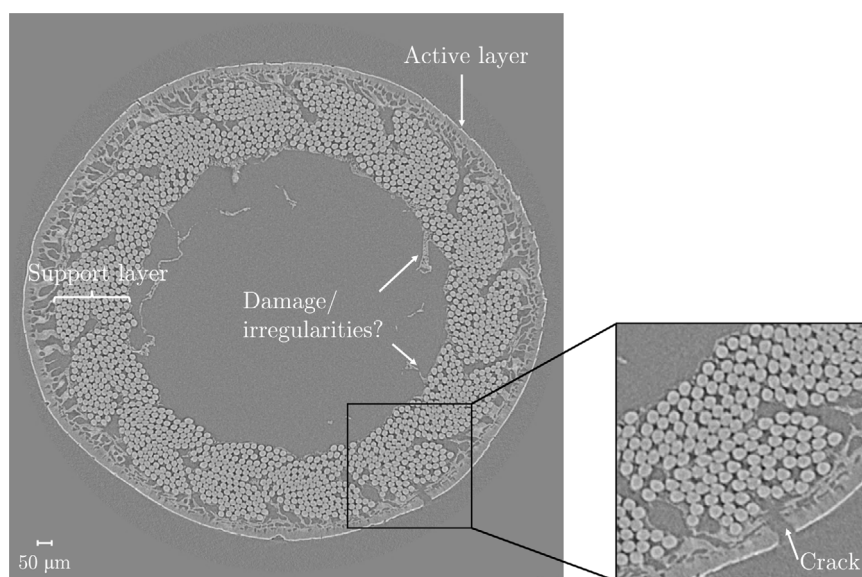


**Fig. 7.** Tomographic cut-slice of a hollow fibre UF membrane.

volume of both decreased with increasing KCl concentration, while macro-voids increased in volume with an increase in KCl concentration. Moreover, compared to the pristine membranes, more macro-voids were detected in the swollen and subsequently dried membranes. In a later study, the same group combined chronopotentiometry with  $\mu$ CT to investigate the ion transport and the heterogeneity in heterogeneous ion-exchange membranes and compared this to single ion-exchange resin particles [32].

Lab-based  $\mu$ CT has further been used in several studies to investigate membrane fouling of polymeric membranes. Löwer and co-workers [33–35] have used the technique to evaluate and describe multiphase processes in a filter cake. They investigated structural parameters such as porosity, tortuosity, and capillary length to develop a model describing the dewetting of a filter cake. Luo et al. [36] characterised membrane fouling on forward osmosis membranes used in an osmotic membrane bioreactor. Lab-based  $\mu$ CT was used to visualise the fouling layer while synchrotron light-based infrared mapping was applied to identify its chemical composition. The membrane was a commercial thin film composite membrane consisting of a polyamide

selective layer with aquaporin protein vesicles embedded and a porous polysulfone support layer (Aquaporin FO, Aquaporin Asia, Singapore, Singapore). The membrane was fouled with activated sludge from a conventional membrane bioreactor. A 0.5 M NaCl solution was used as draw solution. The membrane samples had a diameter of 22 mm and were cut in 10 µm thick slices with a microtome. The generated imaging data were phase retrieved and a voxel size of 1.2 µm was reached. The infrared mapping revealed a multilayer fouling structure with polysaccharide-like substances forming an initial layer that was covered with protein-like substances. Rendering of the data in 3D revealed characteristic “sand-dune” like features as the fouling layer. It was possible to relate these feature to both carbohydrates-like and proteins-like substances.

Fouling of UF membranes due to the filtration of lignocellulosic hydrolysis liquor was investigated by Li et al. [37]. In this work, lab-based  $\mu$ CT was used to visualise the fouling layer and to qualitatively compare a pristine membrane with the fouled membrane. In an unpublished study by the authors, two tubular polyethersulfone UF membranes (ES404, PCI Membranes, now part of Filtration Group, Fareham, UK)

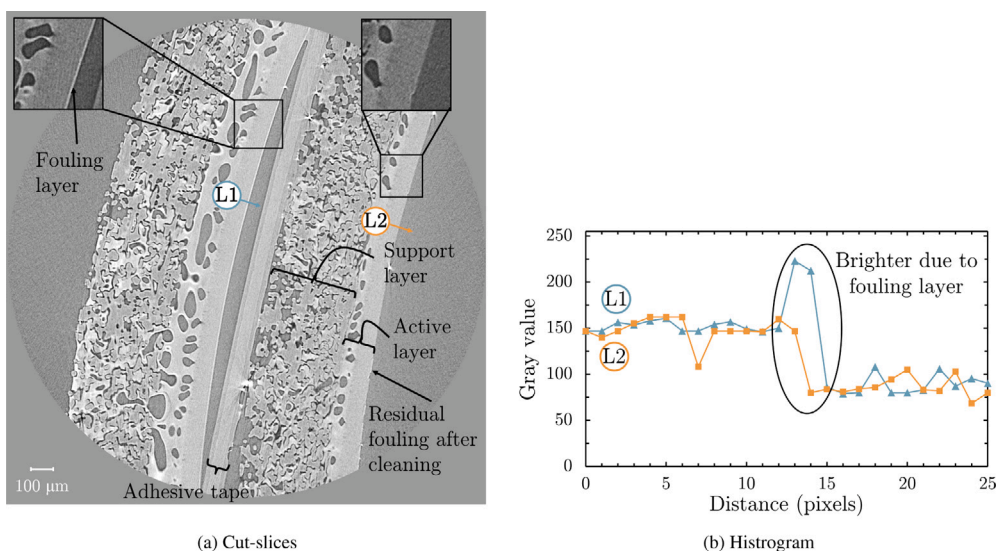


**Fig. 8.** (a) Reconstructed tomographic slices of fouled (left) and cleaned (right) tubular UF membranes. (b) Line profiles of the brightness along the surface of the two imaged tubular membranes.

with a MWCO of 4 kDa were imaged by lab-based  $\mu$ CT (Xradia Versa 520) (Zeiss, Oberkochen, Germany) at the 4D Imaging Lab at Lund University at 80 keV and compared. Both tubular membranes were used for the filtration of bleach plant effluent from softwood pulping. One of them was additionally cleaned with the alkaline cleaning agent BanUltra 17 (Banmark Oy, Vanda, Finland). Details on the preparation can be found in Rudolph et al. [38]. The filtration led to severe membrane fouling that accumulated on the membrane surface. It was possible to uncover the fouling layer as a thin white line on top of the active layer surface, Fig. 8. In the figure, the white line has nearly completely disappeared in the cleaned membrane showing that alkaline cleaning successfully removed the fouling layer. From other analysis it was known that the fouling layer was roughly 2.5  $\mu$ m thick and consisted of magnesium (Mg) [Rudolph, 2021]. As Mg absorbs more X-rays than the membrane polymer, the fouling layer was brighter and easier to detect.

Exploiting phase contrast in combination with phase retrieval additionally to absorption contrast can be used to extract even more information from tomographic X-ray imaging. To fully use the potential of phase-contrast imaging, it is necessary to calculate an image that is predominated by the real part of the complex refractive index and without the edge effects also known as phase retrieval. In Fig. 9, two samples of a UFX5-pHt membrane are shown (unpublished work by the authors). The data were acquired using the Xradia Versa 520 (Zeiss, Oberkochen, Germany) at the 4D Imaging Lab at Lund University at 60 keV with a voxel size of 1  $\mu$ m in the reconstructed 3D images. See Fig. 6(a) for the 3D rendering of the fouled sample. The top one of the two membranes is in pristine state and was only conditioned with a solution of the alkaline cleaning agent Ultrasil 10 (Ecolab, Monheim Germany), the bottom membrane was used for dead-end filtration of thermomechanical pulping process water from spruce (Stora Enso Kvarnsveden, Kvarnsveden, Sweden) at 2 bar and at a temperature of 70°C. For details on the conditioning and filtration, see Virtanen et al. [12]. The finger-like structure in the active layer is clearly visible and easily distinguishable from the non-woven support layer. In the attenuation based slice reconstruction (left side in Fig. 9) both, the pristine and the used membrane seem to be similar. However, after phase-retrieval (right side), spots in the active layer of the used membrane turned bright. Most likely, these bright spots originate from compounds adsorbed on and inside the active layer of the membrane. It can be assumed that these compounds are lignans as they are known to be a severe foulants in membrane processes in pulp and paper processes

and are very small. Therefore they would be able to pass through the pores and adsorb in the active layer.

Not only adsorptive fouling and cake formation can be investigated with lab-based  $\mu$ CT, but also the formation of a biofilm. Davit et al. [39] studied this formation on porous media with the purpose to develop a method for imaging the formation process *in situ*. This study is based on a similar study performed with synchrotron radiation X-ray  $\mu$ CT (SR $\mu$ CT) by Iltis et al. [40]. Davit et al. modelled the pore network in porous media by compressing expanded polyamide beads (1000–3000  $\mu$ m in diameter) between two plexiglas plates. A contrast agent consisting of a medical suspension of barium sulphate ( $\text{BaSO}_4$ ) and potassium iodide (KI) was used to differentiate between the media, the biofilm, and the aqueous phase, Fig. 10. The topologies of the pore-scale transport processes were investigated. A resolution of 9  $\mu$ m was reached. The authors stated that with this approach, a method for imaging biofilm growth within porous media has been established.

### 3.1.2. Synchrotron radiation X-ray radiography

In 2005, Yeo et al. [41] were the first to use synchrotron X-ray imaging for membrane science. In their study, membrane fouling on polymeric membranes was investigated. However, instead of tomographic imaging, they used phase contrast X-ray radiography over time, at the port 16 beamline at the Singapore Synchrotron Light Source, (SSLS), Singapore. In contrast to tomography, in radiography, the sample is not rotated and stands still. Thus, only one projection is extracted. The approach was used to monitor external and internal cake layer deposition on a single polyacrylonitrile hollow fibre MF membrane over time. To improve contrast between the membrane polymer and the solution, an iron hydroxide suspension was used as lumen feed. Due to the low X-ray energy used (10 keV), radiographic images of the internal structure of the membrane were obtained only when the membrane was dry. By this, it was possible to detect a cake layer build up inside the lumen and fouling within the membrane structure. Thus, this study is the first to assess fouling of a metal oxide contamination on membranes using a synchrotron light source. The resolution reached was 1  $\mu$ m.

### 3.1.3. Synchrotron radiation X-ray microtomography

To-date, membrane fouling is still a problem and in a more recent study, a way to decrease the impact of fouling of polymeric UF membranes was investigated with SR $\mu$ CT by Abdelrasoul et al. [42]. The authors investigated the influence of cross-flow air injection to shear of a cake layer during UF. The experiments were done at the biomedical imaging and therapy (BMIT) beamline at the Canadian

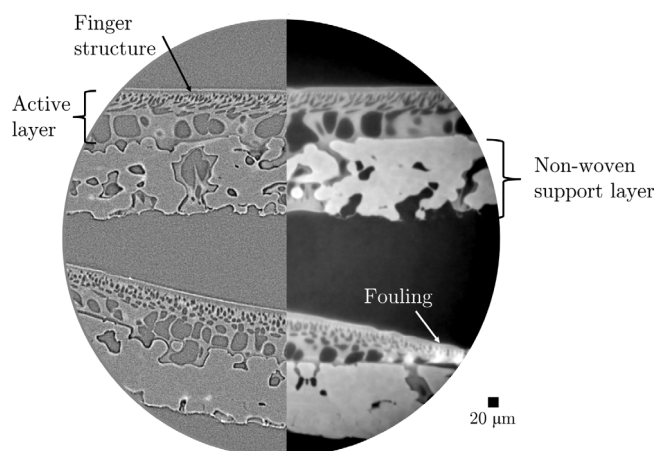


Fig. 9. Non-phase retrieved (left) and phase retrieved (right) lab-based  $\mu$ CT reconstructed tomographic slices of a pristine (top) and a used (bottom) UF membrane.

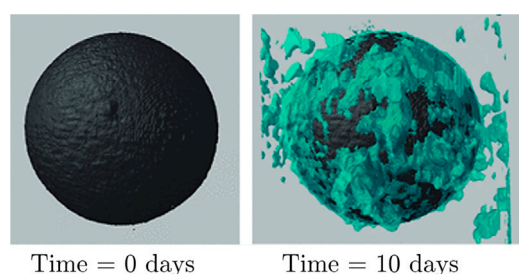


Fig. 10. 3D reconstructions of a polyamide bead (dark) and the biofilm (soft blue-green) at 0 days and after 10 days. (For interpretation of the references to colour in this figure legend, the reader is referred to the web version of this article.)  
Source: Adapted from [39].

© 2010 with permission of John Wiley & Sons, Inc.

Light Source (CLS, Saskatoon, Canada). In-plane imaging was done with the membrane being parallel to the beam path. Two homogeneous polycarbonate membranes with pore sizes of  $0.05\ \mu\text{m}$  and  $0.1\ \mu\text{m}$  and one heterogeneous polysulfone membrane with a MWCO of 60 kDa were used. Fouling was imitated with a concentration of  $1.3\ \text{kg m}^{-3}$  latex particles in an aqueous solution. Air was injected concurrently and counter-currently on the membrane surface at  $0.8\ \text{m s}^{-1}$  while a transmembrane pressure of 1.72 bar (25 psi) was applied. It was possible to reveal the influence of the air injection on the membrane fouling in each membrane layer of the polysulfone membrane matrices. At the top layers, counter current air flow resulted in the removal of membrane fouling, but in the intermediate and lower layers of the polysulfone membrane severe fouling was found. A similar effect was observed for concurrent air injection, but in this case the fouling in the bottom part of the membrane was less severe. The experimental results were supported by an analysis with computational fluid dynamics and additional confocal laser scanning microscopy.

Ceramic membranes have also been investigated with SR $\mu$ CT. Molahosseini et al. [43] monitored the filtration of skimmed milk and combined the findings with molecular dynamics simulations. Variations in porosity and membrane fouling were investigated through different layers from the top, middle, and bottom of cylindrical membranes before, during, and after skimming milk. The membrane had a pore size of  $0.14\ \mu\text{m}$ . In-plane imaging was conducted at the BMIT 05ID-2 beamline of the CLS. A polychromatic beam (white beam) was used and the beam was aligned in a cross-flow direction, thus parallel to the membrane support. Defects in the membrane structure were detected and a homogeneous distribution of the porosity along the thickness of

the membranes was revealed. Fouling was found to be more intense on the top of the membranes even though the top layer was slightly more porous than the lower part. Vicente et al. [44] compared new and used ceramic MF membranes regarding changes of their inner structure in 2D and 3D. The experiment was conducted on the ID19 beam line at the European Synchrotron Research Facility (ESRF), Grenoble, France. Consecutive image analysis of the reconstructed tomographic slices allowed to determine the local thickness variation of the membrane from the feed to the permeate side. Furthermore, a morphological analysis of the solid structure and the pore space was conducted. The 2D characterisation enabled a quantification of the pores before and after filtration, while the 3D characterisation revealed the granulometric distribution of different solid parts of the porous matrix across the thickness of the membrane.

Furthermore, SR $\mu$ CT was applied to determine the morphology of membranes. Remigy et al. [45,46] used SR $\mu$ CT to assess and characterise morphological features and the 3D architecture of polyvinylidene difluoride hollow fibre MF membranes. Also here the ID19 beamline at ESRF was used. The membranes investigated were prepared by phase inversion through different manufacturing processes. The hollow fibres had a length of 3 to 4 cm. The samples were in wet state and no sample preparation was conducted. During the experiment, about  $750\ \mu\text{m}$  of the hollow fibres were scanned. A voxel size of  $0.7\ \mu\text{m}$  was achieved. The study showed that the hollow fibres consisted of four regions distinguishable from each other by the pore wall thickness and pore size distribution. Additionally, density differences in the polymer walls were detected.

Even transport phenomena related to membrane processes can be studied with SR $\mu$ CT. Park et al. [47] applied the technique with a white beam to monitor the separation of water-in-oil emulsions on the microscale. Under-oil-hydrophilic membranes, a conventional non-woven filter paper with a pore size of around  $20\ \mu\text{m}$ , was used. The sample was placed in a chamber filled with an oil phase. Then a droplet of an aqueous solution consisting of iodine and KI was dispensed into the chamber to investigate the early stage of the spreading and adsorption of water droplets on the filter paper. The experiment was conducted at the 9D beamline of the Pohang Light Source (PLS-II, Pohang Accelerator Laboratory, Pohang, South Korea). It was found that not only membrane characteristics but also fluidic interactions between the water and the oil phase significantly affected the dynamic behaviour of the water droplets in the overall separation process. Just recently, the same authors reported a 4D visualisation of the process by using *operando* SR $\mu$ CT at the 6C Bio Medical Imaging beamline of PLS-II [48]. In this study, the reached voxel size was around  $2.25\ \mu\text{m}$ . Correcting for edge effects using phase retrieval made it possible to

study the spatial-temporal volume changes of the oil–water phase and the variation of pore distribution within the hydrophilic membrane in 3D. The investigations made it possible to calculate the volume flow rate of oil infiltrating the filter paper and the evaporation rate of water from the filter paper. Overall, the work showed that oil adsorption is a result of a competition between capillary action caused by water evaporation and oil infiltration pressure caused by surface wettability changes. Another example on the usage of *operando* SR $\mu$ CT for transport phenomena is the observation of water transport in polymer electrolyte fuel cells done by Normile et al. [49]. With the help of a combination of SR $\mu$ CT and full-field X-ray nCT, the formation of liquid water around the interface of components of the fuel cell and within larger voids in the catalyst layer was observed. Preliminary runs were performed at the Beamline 2-BM at the Advanced Photon Source (APS) hosted at the Argonne National Laboratory (ANL, Argonne, IL, USA), while the final experiment was run at the Beamline 8.3.2 at the Advanced Light Source (ALS) hosted at Lawrence Berkeley National Laboratory (LBNL, Berkeley, Ca, USA). Findings from this study can be used to improve the design of electrodes and component interfaces of fuel cells with regards to water management and power density.

### 3.2. X-ray holotomography in membrane science

Holotomography, i.e., in-line holography combined with tomography and also known as projection microscopy, is a lensless coherent nanotomographic X-ray imaging technique that exploits the coherent flux of high-brilliance X-ray sources. Holotomography and in-line holography, as developed by Gabor [50], provide phase information by interfering a reference wave with the one distorted by the sample. In a magnified geometry using a focused beam, as in projection microscopy [51], the resolution of in-line holography and holotomography is limited by the focal spot size of the focused beam. Given the advent of diffraction-limited storage rings [52] and high-resolution X-ray optics, sub-100 nm focusing has become a routine task [53,54] and even close to few tens of nanometres [55,56]. Thus, holotomography is an excellent technique to probe the mesoscale, i.e., 100 nm resolution down to the nanometre scale with phase sensitivity with a field-of-view around hundreds of micrometres.

For example, in a recent in-line holography experiment at the MAX IV Laboratory synchrotron light source hosted at Lund University, (Lund, Sweden) the capabilities of the NanoMAX beamline [57] were demonstrated on a chalk sample and a spatial resolution of 155 nm was achieved in a scan time of few minutes [54].

Until now, holotomography has not yet been applied for studies related to membrane science, but it has already been successfully used for soft matter such as bio-molecular structures and metal thin films [58]. This technique is foreseen to be a very promising method for membrane science as it shows high sensitivity, requires short measuring times, and allows low-dose imaging, meaning less beam damage [54]. The aforementioned properties are especially useful when imaging objects made of low-atomic-number (Z) chemical elements such as hydrogen (H), carbon (C), and oxygen (O) and materials with similar attenuation contrast typically associated to polymeric membranes and organic membrane fouling.

### 3.3. Full-field X-ray nanotomography in membrane science

Synchrotron radiation full-field nCT, also known as transmission X-ray microscopy (TXM) is using phase contrast for imaging similar to  $\mu$ CT but can additionally employ refractive lenses, Fresnel zones plates, or Zernike phase contrast [14,59]. The technique has been used in two studies related to membrane science. It was used to characterise the spatial distribution and 3D shape of macrovoids in bicontinuous microemulsion-fabricated polymeric films [60]. The polymeric films modelled the nanoporous structure of membranes. Three films were prepared by thermal polymerisation. The films consisted

of 2-hydroxyethyl methacrylate used as the aqueous component of each micro-emulsion, ethylene glycol dimethacrylate used as cross-linking agent. N,N,N',N'-tetramethylethylene diamine together with ammonium persulfate were used for the polymerisation. One film was prepared by UV cross-linking of a silicon monomer. Each sample had a size of  $50 \times 80 \mu\text{m}^2$  and was put in a capillary for imaging. The experiment was conducted at the 7C beamline of the PLS-II using a monochromatic X-ray beam. A resolution of around 40 nm was reached. It was possible to visualise the 3D morphology, pore channels, and pore inter-connectivity across the polymeric films. Furthermore, it was possible to quantify the tortuosity and porosity of the polymeric films. As mentioned before, Normile et al. [49] conducted a study where they used a combination of SR $\mu$ CT and *operando* full-field nCT to investigate the formation of liquid water in polymer electrolyte fuel cells. Samples at different relative humidities (50% and 100%) were studied and ionomer (polymers consisting of repeat units of electrically neutral repeating units and a fraction of ionised units) swelling was observed within macro-pores smaller than 1  $\mu\text{m}$ . The experiments were conducted at the 32-ID Beamline at APS. A field of view of  $75 \times 75 \mu\text{m}$  was used and the scan time was approximately 20 min. A resolution of 60 nm was achieved.

### 3.4. Ptychographic X-ray computed tomography for membrane science

PXCT is a coherent lensless imaging technique that bypasses limitations in quality and resolution of conventional imaging lenses by relying on computational reconstructions [61,62]. The sample of interest is scanned across an X-ray beam, ensuring sufficient overlap between the illuminated regions, and, for each scanning position, a far-field diffraction intensity pattern is measured. Due to the phase-retrieval reconstruction, the resolution in the reconstruction is not limited by either the scanning step size nor by the diameter of the illumination.

For 3D nanoscale imaging, ptychograms of the sample can be acquired at different sample orientations with respect to the direction of beam propagation [63,64]. PXCT leverages the improved signal of phase contrast at high X-ray energies, compared to absorption contrast, and, if the incident photon energy is away from resonant edges of the sample, while providing quantitative 3D electron density maps [65]. Currently the typical resolution achievable is around 20 nm, although the technique continues to be actively developed and has substantial room for higher resolutions.

PXCT has so far been reported once for membrane science to determine the 3D structure of four commercial state-of-the-art polytetrafluoroethylene (PTFE) membranes used in membrane distillation [66]. The membrane samples investigated were FGLP14250, FHLP14250, FGLP14250 from Merck Millipore, Burlington, MA, USA and Gore from W. L. Gore and Associates, Newark, DE, USA. Their pore sizes varied between 0.2 and 0.45  $\mu\text{m}$ . PXCT was conducted at the cSAXS beamline of the Swiss Light Source (SLS) at the Paul Scherrer Institute (PSI), Villigen, Switzerland. A spatial resolution between 82 and 128 nm was reached. The porosity, tortuosity, and permeability of the membranes were determined. It was found that the porosity for the three samples agreed well with the values stated by the two manufacturers. However, an inhomogeneous distribution of porosity along the membrane thickness was observed for all three samples. The determined characteristics were used for a numerical simulation comparing permeability and Knudsen effects of the membranes with the dusty gas model. To generate a better understanding of the pore network and the membrane morphology, it was proposed to conduct a structural analysis and to determine the pore size distribution and mean pore size of the membranes.

In a study under preparation, the authors have used PXCT at the cSAXS beamline of SLS to investigate membrane fouling of MF and UF membranes. Images were acquired at 6.2 keV. The scan time was around 6 h for a total of 1050 projections. A resolution of 26.5 nm was

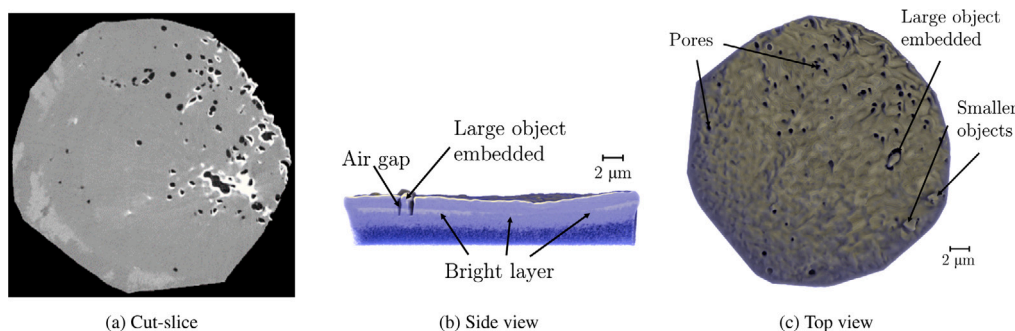


**Fig. 11.** Reconstructed tomographic slice (a) and 3D rendering of a UF membrane used for the separation of lysozyme from a fermentation broth seen from the side (b) and the top (c).

reached in the reconstructed 3D images. Amongst the UF membranes a GR60PP membrane (Alfa Laval, Naskov, Denmark) made from polysulfone and with a MWCO of 20 kDa was imaged. This membrane was used for the separation of the protein lysozyme (Lysozyme, from chicken egg white, Alfa Aesar, Haverhill, MA, USA) from a fermentation broth to model the downstream processing of a sweet protein produced by precision fermentation. The broth had a concentration of  $1 \text{ g L}^{-1}$  lysozyme. UF was run in a stirred dead-end cell with a volume of 350 mL at  $30^\circ\text{C}$ , 2.0 bar transmembrane pressure, and 500 rpm stirring rate, until a volume reduction of 50% was reached. The filtration reduced the membrane's pure water permeability to 26% of the initial value indicating severe membrane fouling.

In the 3D rendering of the sample, a fouling layer is visible on top of the membrane, Fig. 11. In the upper part of the side view (Panel (b) in Fig. 11), a roughly 400 nm thick bright layer can be seen. This presumably originated from locally precipitated minerals and is most likely located just on top the active layer of the membrane. On the left side in the same panel, a large object is visible that seems to be embedded in the fouling layer and enclosed by a gap. From the top view (Panel (c) in Fig. 11), it can be seen that the fouling layer is not homogeneous. Pores are visible and the large object clearly stands out. The previously described gap around the large object is also visible. Furthermore, several smaller objects are embedded in the top layer. So far, it can only be speculated what these objects might be. The large object could be a cell of a contaminant. The gap around it might be from this microorganism consuming parts of the fouling layer. The smaller objects could either be dust that ended on the surface during preparation or precipitated compounds from the fermentation broth. Investigations with further complementing techniques are needed to outline and confirm these observations.

#### 4. Opportunities, challenges, and limitations

##### 4.1. Opportunities

Tomographic X-ray imaging techniques offer the possibility to uncover many fundamental issues related to membrane science that are to-date not fully understood. Especially the different foci and achievable resolutions allow to image structures at various length- and time-scales. This is very useful for hierarchical structures such as membranes. A summary of key properties relevant for imaging by tomographic X-ray imaging techniques can be found in Table 1. The table shows the possibilities of these techniques. It needs to be explored to what extent the presented values can be achieved when imaging membranes, membrane modules, or membrane processes.

Tomographic X-ray imaging techniques can be used for rapid macroscopic quality control during the production of membranes, their integration in a module and in its housing, and their behaviour during operation. Especially lab-based  $\mu\text{CT}$  is valuable for such rapid analysis, as it is readily available while still allowing for measurements within a

sample environment. However, imaging at a synchrotron light source would be much faster.

Already with lab-based instruments, flow conditions inside a membrane module can be monitored [25]. Observing flow conditions can be used to improve the module design or to develop new modules, e.g. dead-spots in the modules could be detected. Also, the optimisation of spacers or the development of novel spacer designs can be promoted with *operando* tomographic imaging of the flow patterns. Monitoring the flow of liquids can be improved when the contrast is enhanced. One way of achieving this is the usage of contrast agents, see the work of Frank et al. [25] as it is already standard in medical imaging. A disadvantage of this approach might be that the contrast agent interacts with the membrane. Another approach can be the combination of tomographic X-ray imaging with tomographic neutron imaging as it was done by Maier et al. [30]. Neutrons can enhance the contrast of a sample when water ( $\text{H}_2\text{O}$ ) is replaced with heavy water ( $\text{D}_2\text{O}$ ). Meaning, the membrane has to be filled with  $\text{D}_2\text{O}$  first. Then, 2D/3D imaging by neutrons can be started and the replacement of  $\text{D}_2\text{O}$  with  $\text{H}_2\text{O}$  can be monitored. Another example on the usage of neutrons is the imaging of the fluid flow in rock [74], an approach that could be easily transferred to similar investigations on ceramic membranes.

Macroscopic biofilm formation, scaling, and cake build-up can be detected and monitored *in situ* with tomographic X-ray imaging [39]. The high resolutions reached with nanotomographic X-ray imaging techniques enable pore characterisations of, e.g., MF or open UF membranes. Thus, they allow investigations of cake formation, pore blocking, and adsorptive fouling during/after filtration and/or cleaning. When doing this, it is possible to conduct a detailed pore size analysis that also includes isolated pores, which might be disconnected by membrane fouling or scaling. This is a substantial advantage compared to other methods for pore analysis such as physisorption or mercury porosimetry. The combination of tomographic X-ray imaging with other techniques for further (chemical) analyses of the sample could give detailed information on compounds adsorbed on and in the membrane.

At synchrotron light sources, the brilliance of the X-ray beams can be so high that high temporal resolutions are possible and even fast changes of or in the sample could be monitored. For example, it has been shown that complex systems such as a pumping heart can be studied by tomographic X-ray imaging to learn about flow conditions inside the organ [75]. This ability of synchrotron radiation could be useful to learn about the complex processes connected to the phase-transition in membrane distillation or the transition of ions between the anion and cation exchange layer in bipolar ion-exchange membranes in electrodialysis. Furthermore, with high temporal resolutions, many samples can be imaged during one beamtime, which would allow to run larger studies or to investigate more samples of the same type to get a better reliability of the analysis.

**Table 1**

Overview of record parameters for the full-field tomographic X-ray imaging techniques micro-, holo-, nanotomography, and ptychotomography. The presented values are reported records of the techniques. These values were achieved on samples not related to membrane science and are only to a limited extend transferable to membrane science (yet).

Technique	Resolution	Field of view (h×v)	Temporal resolution	Availability
Microtomography	> 0.7 $\mu\text{m}$	>100 × 100 $\text{mm}^2$	<1 ms [67,68]	Lab, SR
Holotomography	100 nm [54,69]	<20 × 20 $\mu\text{m}^2$ [54]	25 ms [69]	Lab, SR
Nanotomography	> 10 nm [70]	60 × 60 $\mu\text{m}^2$ [14,70]	33 ms [71]	Lab, SR
Ptychotomography	> 15 nm [64,72]	<100 × 100 $\mu\text{m}^2$ [73]	100 ms [64]	SR

h×v: horizontal × vertical, Lab: Lab-based X-ray source, SR: Synchrotron radiation.

#### 4.2. Challenges

One of the biggest challenge for using tomographic methods for membrane science is probably the access to X-ray sources for performing tomographic experiments, both laboratory-based and at a synchrotron light source. However, more and more university labs are acquiring lab-based X-ray sources for tomography. These instruments are often open for anyone by establishing a collaboration or through a proposal that is reviewed by an external committee of experts.

For tomographic techniques using synchrotron light sources, a key question is to identify the right beamline, and to apply for and receive granted beamtime. All beamlines have different specifications, advantages, and disadvantages. The effort to identify which technique would be the most suitable one for a given experiment in mind should not be underestimated. For getting beamtime, a proposal has to be prepared and submitted. It is recommend to contact and consult the beamline scientist before writing a proposal. In the proposal, the goal and scientific motivation of the experiment has to be clearly stated and it should be evident that the team of proposers have the necessary expertise to carry out the experiment, to analyse the results and that the experiment actually will be able to answer a clearly stated scientific hypothesis. It is wise to include results from preliminary/previous tomographic experiments in the proposal, which helps not only to become acquainted with the method but also to develop a suitable experimental plan, to demonstrate the proposers' knowledge on the technique, and, ideally, to establish a data processing pipeline. Due to the described efforts needed for tomographic imaging at a synchrotron light source, is important to rule out that lab-based CT could solve the questions too.

Luckily, synchrotron light sources are increasingly more accessible. Table 2 gives an overview of synchrotron light sources worldwide with beamlines offering tomographic X-ray imaging. Several additional synchrotrons are currently under construction; examples are the Iranian Light Source Facility (ILSF), the Turkish Accelerator Radiation Laboratory (TARLA), and the Synchrotron-Light for Experimental Science and Applications in the Middle East (SESAME) in Jordan. Funding for more synchrotron light sources is considered as those facilities are high in demand and produce top-notch science; an example is the African Light Source which would be the first synchrotron light source on the African continent. In general, most synchrotron light sources have at least one tomography beamline since X-ray tomographic imaging is an important analysis method. At SESAME an imaging beamline called BEAmline for Tomography at SESAME (BEATS) was just recently inaugurated. It is most likely that the ILSF and TARLA will have tomography beamlines too.

When granted, a beamtime slot at a synchrotron light source usually covers the costs for the experiment including support by a beamline scientist(s). However, the beamtime is often limited to a few days per set of experiment. A challenge is that sample preparation for certain experiments, especially when a high resolution is targeted, is often time-consuming and cost-intensive. Often, the sample needs to be tiny for high resolution imaging. A typical method for standardised sample preparation of such samples is abrasion with an ion beam (FIBing). Samples can than be attached to, e.g. OMNY pins [76]. OMNY stands for tOMography Nano crYo and is an instrument at the cSAXS beamline

at SLS, PSI whose sample mounting pins have become a standard also for many other beamlines, as it allows interchange and re-imaging at several beamlines. Usually, the proposers have to cover the costs for sample preparation themselves and this should ideally be considered already in the stage of the project funding proposal. Efforts to alleviate the costly process of sample preparation are in development. Holler et al. developed a lathe system for micrometre-sized cylindrical sample preparation at room and cryogenic temperatures [77]. For now, this might be useful for samples of ceramic membranes.

Another essential challenge regarding tomographic X-ray imaging arises after the experiment has been conducted. Then, the projection images have to be postprocessed and/or reconstructed. Thereafter, reconstructed tomographic slices of the sample need to be processed (image processing), analysed, (image analysis), quantified, and visualised. Fig. 12 presented a standard procedure for performing tomographic X-ray imaging experiments related to membrane science proposed by us. In the procedure, we showed that most of the tasks are not to be done alone by the membranologist but most likely with the help of tomography or sample preparation experts. The procedure starts with preparing a membrane or a membrane module by producing, mounting, or using it. This depends on the aim of the study and is most likely driven by the membranologist. However, already here, it is wise to consult a tomography expert to adjust the experiment according to the tomographic instrument. Thereafter, the sample or the entire module needs to be mounted on a sample holder. Then, the imaging experiment will take place. Both steps need the expertise of membranologists, sample preparation and tomography experts. Often reconstruction of the data set into tomographic slices is done in-house at the synchrotron light source with the help of the tomography expert. Thereafter, image processing, image analysis, quantification and visualisation is performed. For this, extensive knowledge is crucial. Therefore, also for these last tasks, it is wise to reach out to experts to be able to extract as much information as possible from the generated data sets.

Various software tools can help with image processing, image analysis, and visualisation. Often, there are open-source versions available. Common software tools used in the literature are: Fiji/ImageJ [78] (open-source, National Institutes of Health, USA), Paraview [79], Tomviz (tomviz.org) (both open-source, Kitware, Clifton Park, NY, USA), Drishni [80] (open-source, Australian National University Vizlab, Acton, ACT, Australia), Avizo (commercial, Thermo Fisher Scientific, Waltham, MA, USA), Dragonfly (commercial but a student license is available, Object Research Systems, Montréal, Canada), Ilastik [81] (open-source, Anna Kreshuk's lab at the European Molecular Biology Laboratory, Heidelberg, Germany), Matlab or Python and applicable packages such as SciKit Imaging [82], SciPy [83], PoreSpy [84], pytrax or the tools from the Center for Quantification of Imaging Data from MAX IV (qim.dk) (all for python and open-source). However, one has to be able to identify the right software tool for the questions to be answered.

#### 4.3. Limitations

Perhaps, the most important limitation of tomographic X-ray imaging techniques is the achievable resolution and trade-off between resolution and field of view. For macroscopic phenomena (see Fig. 1) this

**Table 2**

Summary of synchrotron light facilities and beamlines for full-field 3D tomographic imaging with hard X-rays, considering microtomography, nanotomography, holotomography and ptychotomography.

Hosting facility	Synchrotron	Country	Imaging beamlines	Available techniques
Australian Nuclear Science and Technology Organisation (ANSTO)	Australian Synchrotron	Australia	IMBL, MCT, ADS-1, ADS-2	Microtomography
Argonne National Laboratory	Advanced Photon Source (APS)	IL, USA	2-BM-A, 7-BM-B, 32-ID-B, 32-ID-C	Micro- and nanotomography, ptychotomography
Brazilian Synchrotron Light Laboratory (LNLS)	Sirius	Brazil	MOGNO, Caterete	Micro- and nanotomography, ptychotomography
Brookhaven National Laboratory	National Synchrotron Light Source II	NY, USA	3-ID HXN, 9-ID CDI, 18-ID FXI	Micro- and nanotomography, ptychography
Canadian Light Source (CLS)	CLS	Canada	BMIT, SM	Micro- and nanotomography
Center for the Advancement of Natural Discoveries using Light Emission (CANDLE Synchrotron Research Institute)	CANDLE Synchrotron Research Institute	Armenia	3 Medical imaging	Computed tomography
Consortium for the Exploitation of the Synchrotron Light Laboratory (CELLS)	ALBA	Spain	BL09 - MISTRAL	Micro- and nanotomography
Cornell University	Cornell high Energy Synchrotron Source	NY, USA	Structural Materials Beamline	Microtomography
Deutsches Elektronen-Synchrotron (DESY)	PETRA III	Germany	P05, P06, p07, P21.2	Micro- and nanotomography, ptychotomography
Diamond Light Source	Diamond Light Source	UK	K11 DIAD, I12 JEEP, I13, B24	Microtomography, ptychotomography
Elettra Sincrotrone Trieste	Elettra Sincrotrone Trieste	Italy	SYRMEP	Microtomography
European Synchrotron Research Facility (ESRF)	ESRF	France	ID19, BM18, ID17, BM05	Microtomography
Helmholtz Zentrum Berlin (HZB)	BESSY-2	Germany	BAMLine	Microtomography and holotomography
Institute of High Energy Physics	Beijing Synchrotron Radiation Facility	China	4W1 A	Microtomography
Institute of Physical and Chemical Research (Riken)	SPRING-8	Japan	BL20XU, BL24XU (Hyogo ID), BL28B2, BL29XU, BL47X	Micro- and nanotomography, ptychotomography
Jagiellonian University	National Synchrotron Radiation Centre SOLARIS	Poland	POLYX <sup>a</sup>	Microtomography
Karlsruhe Institute of Technology	ANKA	Germany	TOPO-TOMO	Microtomography
Karlsruhe Institute of Technology	Karlsruhe Research Accelerator (KARA)	Germany	IMAGE	Microtomography
Kurchatov Institute	Kurchatov specialised source of synchrotron radiation (KISI-Kurchatov)	Russia	RT-MT	Microtomography
Kyushu Synchrotron Light Research Center	SAGA Light Source	Japan	07	Microtomography
Lawrence Berkley National Laboratory	Advanced Light Source (ALS)	CA, USA	8.3.2	Microtomography
Louisiana State University	Center for Advanced Microstructures and Devices (CAMD)	LA, USA	5A1	Microtomography
Lund University	MAX IV Laboratory	Sweden	ForMAX, DanMAX, NanoMAX	Micro- and nanotomography, ptychography, holotomography
National Laboratory for Higher Energy Physics	Photon Factory	Japan	AR-NE7 A, BL-14C	Microtomography
National University of Singapore	Singapore Synchrotron Light Source (SSLS)	Singapore	PCIT	Microtomography
National Synchrotron Radiation Research Center (NSRRC)	Taiwan Light Source (TLS)	Taiwan	BL01A1, BL01B1	Micro- and nanotomography
National Synchrotron Radiation Research Center (NSRRC)	Taiwan Photon Source (TPS)	Taiwan	24 A, 27 A	Microtomography, ptychography
Paul Scherrer Institute (PSI)	Swiss Light Source (SLS)	Switzerland	cSAXS, TOMCAT	Ptychotomography, micro- and nanotomography
Pohang Accelerator Laboratory (PAL) and POSTECH	Pohang Light Source-II (PLS-II)	South Korea	6C, 7C	Micro- and Nanotomography

(continued on next page)

Table 2 (continued).

Hosting facility	Synchrotron	Country	Imaging beamlines	Available techniques
Raja Ramanna Centre for Advanced Technology Ritsumeikan University	Indus-2 Ritsumeikan SR center	India Japan	BL-04 BL-12	Microtomography
Shanghai Institute of Applied Physics	Shanghai Synchrotron Radiation Facility (SSRF)	China	BL08U1, BL13W1	Micro- and nanotomography
SLAC National Accelerator Laboratory	Stanford Synchrotron Radiation Lightsource (SSRL)	USA	2-3	Microtomography
Société civile Synchrotron (SOLEIL)	SOLEIL	France	ANTOMIX, PSICHE, SWING	Microtomography, ptychotomography
Synchrotron Light Research Institute (SLRI)	Siam Photon Source (SPS)	Thailand	BL1.2 W	Microtomography

<sup>a</sup> Beamline under construction.

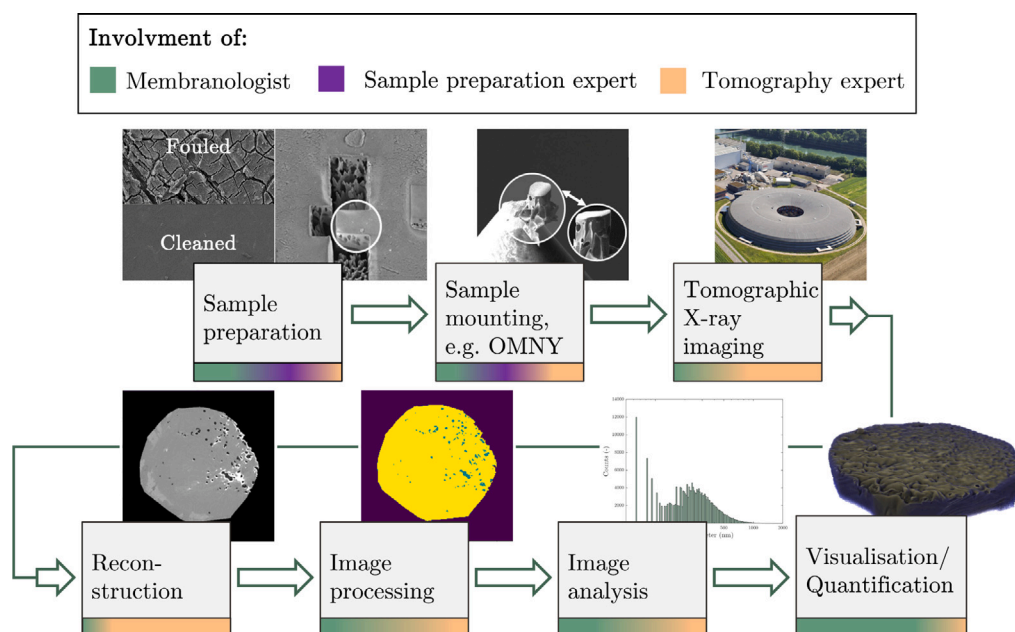


**Fig. 12.** A standard procedure for performing tomographic X-ray imaging experiments related to membrane science. Green: Tasks with involvement of membranologist. Purple: Tasks with involvement of sample preparation expert(s). Orange: Tasks with involvement of tomography expert(s). (For interpretation of the references to colour in this figure legend, the reader is referred to the web version of this article.)

is it not of importance, but e.g., pore analysis is limited to membranes with pore sizes > 20 nm such as MF and open UF membranes. A pore analysis of dense UF, NF, and RO membranes is currently not possible with these techniques. However, this does not exclude the study of phenomena associated to membrane processes with denser pores, such as scaling during desalination, concentration polarisation, or fouling — as demonstrated in the literature review. Another limitation is the relatively small field of view that comes along with the nanotomographic X-ray imaging techniques nCT, holotomography, and PXCT. Thus, it could be questioned if a selected sample region of several micrometre in size is representative for the bulk of the sample. However, a test of representative volume of interest for each technique could give information about this [85]. Moreover, a combination with other methods such as  $\mu$ CT, SAXS or SEM could be considered to assure that the sample is representative. As mentioned before, running an experiment at a synchrotron light source would allow to run many samples of the same type to increase the reliability and representativeness of the analysis.

Another aspect that should be considered is the influence of radiation on the sample. The X-ray beam penetrating through the sample could alter or even damage the sample. This might be a problem for polymeric membranes and delicate fouling layers. However, so far, this point is more hypothetical as beam damage has neither been reported

in the literature nor did we observe it in our own experiments (the unpublished work shown in Figs. 9, 8, and 11.) Overall, the potential risk of beam damage depends on the sample material and the imaging technique applied as well as the exposure time and the energy of the X-rays; lower energies equal longer exposure times which could result in alteration of the sample.

A third limitation is the contrast difference between the membrane and the feed solution. A low contrast can be caused if the membrane contains compounds of similar density as the feed solution, i.e. a polymeric membrane used for separating organic compounds. Here, the usage of contrast agents [25], could be considered to improve the analysis.

Finally, it can be difficult to connect the chemical composition of a sample with the 3D structure determined with tomographic X-ray imaging. However, it is possible to ascribe the contrast seen in X-ray tomographic images to chemical properties but it can be useful to apply supplementary techniques such as spectroscopy to extract more chemical information from a sample. Note that techniques providing elemental information in 3D exists. One is X-ray fluorescence tomography [86,87], a spectrographic imaging technique, which has not yet been applied for membrane science but has quite a potential; another is X-ray infrared mapping, which has for example been used in the

work of Luo et al. for the characterisation of membrane fouling in osmotic bioreactors and identified the distribution of carbohydrates and proteins on the membrane surface [36].

## 5. Conclusions

This work has provided a perspective on the usage of potentially the most suitable tomographic X-ray imaging techniques for the field of membrane science: (i) microtomography, (ii) nanotomography, (iii) holotomography, and (iv) ptychotomography. A background on these four tomographic X-ray imaging techniques was given and studies related to membrane science where these techniques have already been applied were presented.

Tomographic X-ray imaging techniques offer unique information for the field of membrane science. They have several advantages over conventional techniques for structural and mechanical characterisation of membranes, membrane modules, and membrane processes, and provide insight in 3D on a spatial scale never seen before. An important challenge of tomographic X-ray imaging techniques is their accessibility, while an important limitation is their resolution, which is lower than for other microscopic techniques such as AFM, SEM, or TEM. The main advantage is that tomographic X-ray imaging enables non-destructive 3D imaging with the possibility of *in situ/operando* studies and without artefacts from mechanical- or ion-beam-cutting. It needs to be highlighted that collaborations with knowledgeable partners are key for a successful tomographic imaging experiment.

Besides their challenges and limitations, tomographic X-ray imaging techniques hold many opportunities to generate novel knowledge on phenomena related to membrane science that still need understanding. The techniques will not replace established analytical techniques for the characterisation of membranes, but they will serve as important complementary techniques. The development of brighter X-ray sources will allow the advancement of tomographic X-ray imaging techniques away from synchrotron light sources towards lab-based instruments and will make their usage even more widely available, e.g. the Excillum MetalJet anode source, currently the brightest X-ray lab-source in the world. In the near future, tomographic X-ray imaging techniques will become increasingly common analytical techniques for membrane manufacturers, scientists, and users.

## Declaration of competing interest

The authors declare the following financial interests/personal relationships which may be considered as potential competing interests: Gregor Rudolph-Schoepping, Emanuel Larsson, Stephen Hall, and Frank Lipnizki reports financial support was provided by Sweden's Innovation Agency. Gregor Rudolph-Schoepping and Frank Lipnizki reports financial support was provided by EIT Food.

## Data availability

Data will be made available on request.

## Acknowledgements

This work has been performed with support from Sweden's Innovation Agency under the project "Measurements of membrane fouling in lignocellulosic biorefineries by ptychotomography" ref. no. 2019-03613 and EIT Food co-funded by the European Union under the project "Precision Fermentation: From Biotechnology to Sustainable Nutrition, ref. no. 21063. We acknowledge the Paul Scherrer Institute, Villigen, Switzerland for providing of synchrotron radiation beamtime at the beamline cSAXS of the SLS under the proposal 20220560. Furthermore, we acknowledge the support in the image analysis and visualisation provided by the Quantification of Imaging Data from MAX IV (QIM) project at Lund University and the QuantIm hackathon at LINXS (Institute of Advanced Neutron and X-ray Science, Lund, Sweden). Finally, GRS would like to thank The Royal Physiographic Society in Lund for a young research travel grant".

## References

- [1] Grand View Research, Membrane separation technology market size, share & trends analysis report by technology (microfiltration, ultrafiltration, nanofiltration, reverse osmosis), by application, by region, and segment forecasts, 2022 - 2030, in: Market Analysis Report, (no. GVR-4-68038-503-8) 2021, URL <https://www.grandviewresearch.com/industry-analysis/membrane-separation-technology-market>.
- [2] U. Beuscher, E.J. Kappert, J.G. Wijmans, Membrane research beyond materials science, *J. Membr. Sci.* 643 (2022) 119902, <http://dx.doi.org/10.1016/j.memsci.2021.119902>.
- [3] K.C. Khulbe, T. Matsuura, Membrane characterization, in: K.C. Khulbe, T. Matsuura (Eds.), *Nanotechnology in Membrane Processes*, in: Lecture Notes in Nanoscale Science and Technology, vol. 29, Springer, Cham, Switzerland, 2021, pp. 89–133, [http://dx.doi.org/10.1007/978-3-030-64183-2\\_3](http://dx.doi.org/10.1007/978-3-030-64183-2_3).
- [4] J.-C. Remigy, X-ray tomography application to 3D characterization of membranes, in: C. Güell, M. Ferrando, F. López (Eds.), *Monitoring and Visualizing Membrane-Based Processes*, WILEY-VCH Verlag & Co. KGaA, Weinheim, op. 2009, pp. 209–228, <http://dx.doi.org/10.1002/9783527622726.ch10>.
- [5] K.-L. Tung, K.-S. Chang, T.-T. Wu, N.-J. Lin, K.-R. Lee, J.-Y. Lai, Recent advances in the characterization of membrane morphology, *Curr. Opin. Chem. Eng.* 4 (2014) 121–127, <http://dx.doi.org/10.1016/j.coche.2014.03.002>, URL <https://www.sciencedirect.com/science/article/pii/S221133981400029X>.
- [6] Y. Yang, P. Li, X. Zheng, W. Sun, S.X. Dou, T. Ma, H. Pan, Anion-exchange membrane water electrolyzers and fuel cells, *Chem. Soc. Rev.* (2022) <http://dx.doi.org/10.1039/d2cs00038e>.
- [7] M.B. Tanis-Kanbur, R.I. Peinador, J.I. Calvo, A. Hernández, J.W. Chew, Porosimetric membrane characterization techniques: A review, *J. Membr. Sci.* 619 (2021) 118750, <http://dx.doi.org/10.1016/j.memsci.2020.118750>.
- [8] M.A. Islam, M. Ulbricht, Microfiltration membrane characterization by gas-liquid displacement porosimetry: Matching experimental pore number distribution with liquid permeability and bulk porosity, *J. Membr. Sci.* 569 (2019) 104–116, <http://dx.doi.org/10.1016/j.memsci.2018.09.030>.
- [9] J.I. Calvo, A. Bottino, G. Capannelli, A. Hernández, Pore size distribution of ceramic UF membranes by liquid-liquid displacement porosimetry, *J. Membr. Sci.* 310 (1–2) (2008) 531–538, <http://dx.doi.org/10.1016/j.memsci.2007.11.035>.
- [10] A.V. Balyin, A.A. Yushkin, M.N. Efimov, D.G. Muratov, A.V. Volkov, Characterization of porous polyacrylonitrile membranes by liquid-liquid displacement technique, *J. Phys.: Conf. Ser.* 1696 (1) (2020) 012039, <http://dx.doi.org/10.1088/1742-6596/1696/1/012039>.
- [11] B.F. Kingsbury, K. Li, A morphological study of ceramic hollow fibre membranes, *J. Membr. Sci.* 328 (1–2) (2009) 134–140, <http://dx.doi.org/10.1016/j.memsci.2008.11.050>.
- [12] T. Virtanen, G. Rudolph, A. Lopatina, B. Al-Rudainy, H. Schagerlöf, L. Puro, M. Kallioinen, F. Lipnizki, Analysis of membrane fouling by Brunauer-Emmett-Teller nitrogen adsorption/desorption technique, *Sci. Rep.* 10 (1) (2020) 3427, <http://dx.doi.org/10.1038/s41598-020-59994-1>.
- [13] S. Bannwarth, H. Breisig, V. Houben, C. Oberschelp, M. Wessling, Membrane impedance porosimetry, *J. Membr. Sci.* 542 (2017) 352–366, <http://dx.doi.org/10.1016/j.memsci.2017.08.019>.
- [14] A. Takeuchi, Y. Suzuki, Recent progress in synchrotron radiation 3D-4D nano-imaging based on X-ray full-field microscopy, *Microscopy* (Oxford, England) 69 (5) (2020) 259–279, <http://dx.doi.org/10.1093/jmicro/dfaa022>.
- [15] K.P. Brickey, A.L. Zydney, E.D. Gomez, FIB-SEM tomography reveals the nanoscale 3D morphology of virus removal filters, *J. Membr. Sci.* 640 (2021) 119766, <http://dx.doi.org/10.1016/j.memsci.2021.119766>.
- [16] H. Reingruber, A. Zankel, C. Mayrhofer, P. Poelt, Quantitative characterization of microfiltration membranes by 3D reconstruction, *J. Membr. Sci.* 372 (1–2) (2011) 66–74, <http://dx.doi.org/10.1016/j.memsci.2011.01.037>.
- [17] F.H. She, K. Nihara, W.M. Gao, P.D. Hodgson, H. Jinnai, L.X. Kong, 3-Dimensional characterization of membrane with nanoporous structure using TEM tomography and image analysis, *Desalination* 250 (2) (2010) 757–761, <http://dx.doi.org/10.1016/j.desal.2008.11.036>, URL <https://www.sciencedirect.com/science/article/pii/S0011916409010352>.
- [18] X. Wang, D. Huang, B. Cheng, L. Wang, New insight into the adsorption behaviour of effluent organic matter on organic-inorganic ultrafiltration membranes: A combined QCM-D and AFM study, *R. Soc. Open Sci.* 5 (8) (2018) 180586, <http://dx.doi.org/10.1098/rsos.180586>.
- [19] W. Li, X. Liu, Y.-N. Wang, T.H. Chong, C.Y. Tang, A.G. Fane, Analyzing the evolution of membrane fouling via a novel method based on 3D optical coherence tomography imaging, *Environ. Sci. Technol.* 50 (13) (2016) 6930–6939, <http://dx.doi.org/10.1021/acs.est.6b00418>.
- [20] L. Fortunato, M. Li, T. Cheng, Z.U. Rehman, W. Heidrich, T. Leiknes, Cake layer characterization in activated sludge membrane bioreactors: Real-time analysis, *J. Membr. Sci.* 578 (2019) 163–171, <http://dx.doi.org/10.1016/j.memsci.2019.02.026>, URL <https://www.sciencedirect.com/science/article/pii/S0376738818330953>.

- [21] J. Liu, Y. Wang, Z. Li, X. Liu, W. Li, Unraveling relative roles of bulk precipitation and surface growth in developing a scaling layer in membrane distillation, *Desalination* 544 (2022) 116133, <http://dx.doi.org/10.1016/j.desal.2022.116133>.
- [22] H.N. Chapman, K.A. Nugent, Coherent lensless X-ray imaging, *Nat. Photonics* 4 (12) (2010) 833–839, <http://dx.doi.org/10.1038/nphoton.2010.240>.
- [23] D. Paganin, S.C. Mayo, T.E. Gureyev, P.R. Miller, S.W. Wilkins, Simultaneous phase and amplitude extraction from a single defocused image of a homogeneous object, *J. Microscopy* 206 (Pt 1) (2002) 33–40, <http://dx.doi.org/10.1046/j.1365-2818.2002.01010.x>, URL <https://pubmed.ncbi.nlm.nih.gov/12000561/>.
- [24] S. Mohammadi, E. Larsson, F. Alves, S. Dal Monego, S. Biffi, C. Garrovo, A. Lorenzon, G. Tromba, C. Dullin, Quantitative evaluation of a single-distance phase-retrieval method applied on in-line phase-contrast images of a mouse lung, *J. Synchrotron Radiat.* 21 (Pt 4) (2014) 784–789, <http://dx.doi.org/10.1107/S1600577514009333>.
- [25] A. Frank, G. Lipscomb, M. Dennis, Visualization of concentration fields in hemodialyzers by computed tomography, *J. Membr. Sci.* 175 (2) (2000) 239–251, [http://dx.doi.org/10.1016/S0376-7388\(00\)00421-X](http://dx.doi.org/10.1016/S0376-7388(00)00421-X).
- [26] X. Liang, X. Ge, Y. He, M. Xu, M.A. Shehzad, F. Sheng, R. Bance-Soualhi, J. Zhang, W. Yu, Z. Ge, C. Wei, W. Song, J. Peng, J.R. Varcoe, L. Wu, T. Xu, 3D-zipped interface: In situ covalent-locking for high performance of anion exchange membrane fuel cells, *Adv. Sci. (Weinheim, Baden-Württemberg, Germany)* 8 (22) (2021) e2102637, <http://dx.doi.org/10.1002/adv.202102637>.
- [27] J. Vigüé, T. Savart, P. Duru, J.-C. Rouch, J.-C. Remigy, Characterisation of 3D porous macrostructure of hollow fibre membranes using X-ray tomography—Effects of some spinning process conditions, *J. Membr. Sci.* 435 (2013) 11–20, <http://dx.doi.org/10.1016/j.memsci.2013.01.062>.
- [28] G.T. Vladislavljévić, I. Kobayashi, M. Nakajima, R.A. Williams, M. Shimizu, T. Nakashima, Shirasu porous glass membrane emulsification: Characterisation of membrane structure by high-resolution X-ray microtomography and microscopic observation of droplet formation in real time, *J. Membr. Sci.* 302 (1) (2007) 243–253, <http://dx.doi.org/10.1016/j.memsci.2007.06.067>, URL <https://www.sciencedirect.com/science/article/pii/S0376738807004553>.
- [29] A.T. Bridge, M.S. Santoso, J.A. Maisano, A.V. Hillsley, J.F. Brennecke, B.D. Freeman, Rapid macrovoid characterization in membranes prepared via nonsolvent-induced phase separation: A comparison between 2D and 3D techniques, *J. Membr. Sci.* 661 (2022) 120923, <http://dx.doi.org/10.1016/j.memsci.2022.120923>.
- [30] M. Maier, J. Dodwell, R. Ziesche, C. Tan, T. Heenan, J. Majasan, N. Kardjilov, H. Markötter, I. Manke, L. Castanheira, G. Hinds, P.R. Shearing, D. Brett, Mass transport in polymer electrolyte membrane water electrolyser liquid-gas diffusion layers: A combined neutron imaging and X-ray computed tomography study, *J. Power Sourc.* 455 (2020) 227968, <http://dx.doi.org/10.1016/j.jpowsour.2020.227968>.
- [31] M. Svoboda, J. Beneš, L. Vobecká, Z. Slouka, Swelling induced structural changes of a heterogeneous cation-exchange membrane analyzed by micro-computed tomography, *J. Membr. Sci.* 525 (2017) 195–201, <http://dx.doi.org/10.1016/j.memsci.2016.10.046>.
- [32] L. Vobecká, M. Svoboda, J. Beneš, T. Belloň, Z. Slouka, Heterogeneity of heterogeneous ion-exchange membranes investigated by chronopotentiometry and X-ray computed microtomography, *J. Membr. Sci.* 559 (2018) 127–137, <http://dx.doi.org/10.1016/j.memsci.2018.04.049>.
- [33] S. Esser, E. Löwer, U.A. Peuker, Network model of porous media – Review of old ideas with new methods, *Sep. Purif. Technol.* 257 (2021) 1–9, [http://dx.doi.org/10.1016/S1383-5866\(08\)00514-5](http://dx.doi.org/10.1016/S1383-5866(08)00514-5).
- [34] E. Löwer, T. Leißner, U.A. Peuker, Insight into filter cake structures using micro tomography: The dewatering equilibrium, *Sep. Purif. Technol.* 252 (2020) 117215, <http://dx.doi.org/10.1016/j.seppur.2020.117215>.
- [35] E. Löwer, C. Makowlew, T. Leißner, U.A. Peuker, Wetting behavior of porous structures: Three-dimensional determination of the contact angle after filter cake dewatering using X-ray microscopy, *Adv. Water Resour.* 151 (2021) 103894, <http://dx.doi.org/10.1016/j.advwatres.2021.103894>.
- [36] W. Luo, B. Arhatari, S.R. Gray, M. Xie, Seeing is believing: Insights from synchrotron infrared mapping for membrane fouling in osmotic membrane bioreactors, *Water Res.* 137 (2018) 355–361, <http://dx.doi.org/10.1016/j.watres.2018.03.011>.
- [37] S. Li, H. Chen, X. Zhao, L.A. Lucia, C. Liang, Y. Liu, Impact factors for flux decline in ultrafiltration of lignocellulosic hydrolysis liquor, *Sep. Purif. Technol.* 240 (2020) 116597, <http://dx.doi.org/10.1016/j.seppur.2020.116597>.
- [38] G. Rudolph, B. Al-Rudainy, J. Thuvander, A.-S. Jönsson, Comprehensive analysis of foulants in an ultrafiltration membrane used for the treatment of bleach plant effluent in a sulfite pulp mill, *Membranes* 11 (3) (2021) <http://dx.doi.org/10.3390/membranes11030201>.
- [39] Y. Davit, G. Iltis, G. Debenest, S. Veran-Tissoires, D. Wildenschild, M. Gerino, M. Quintard, Imaging biofilm in porous media using X-ray computed microtomography, *J. Microscopy* 242 (1) (2011) 15–25, <http://dx.doi.org/10.1111/j.1365-2818.2010.03432.x>.
- [40] G.C. Iltis, R.T. Armstrong, D.P. Jansik, B.D. Wood, D. Wildenschild, Imaging biofilm architecture within porous media using synchrotron-based X-ray computed microtomography, *Water Resources Res.* 47 (2) (2011) <http://dx.doi.org/10.1029/2010WR009410>.
- [41] A. Yeo, P. Yang, A.G. Fane, T. White, H.O. Moser, Non-invasive observation of external and internal deposition during membrane filtration by X-ray microimaging (XMI), *J. Membr. Sci.* 250 (1–2) (2005) 189–193, <http://dx.doi.org/10.1016/j.memsci.2004.10.035>.
- [42] A. Abdelrasoul, H. Doan, A. Lohi, N. Zhu, Synchrotron based micro tomography (SR-μCT), experimental, and computational studies to investigate the influences of cross flow air injection in ultrafiltration process, *J. Environ. Chem. Eng.* 9 (1) (2021) 104611, <http://dx.doi.org/10.1016/j.jece.2020.104611>.
- [43] A. Mollahosseini, K. Min Lee, A. Abdelrasoul, H. Doan, N. Zhu, Innovative in situ investigations using synchrotron-based micro tomography and molecular dynamics simulation for fouling assessment in ceramic membranes for dairy and food industry, *Int. J. Appl. Ceramic Technol.* 18 (6) (2021) 2143–2157, <http://dx.doi.org/10.1111/ijac.13824>.
- [44] J. Vicente, Y. Wyart, P. Moulin, Characterization (two-dimensional- three-dimensional) of ceramic microfiltration membrane by synchrotron radiation: New and abraded membranes, *J. Porous Media* 16 (6) (2013) 537–545, <http://dx.doi.org/10.1615/JPorMedia.v16.i6.50>.
- [45] J.-C. Remigy, M. Meireles, Assessment of pore geometry and 3-D architecture of filtration membranes by synchrotron radiation computed microtomography, *Desalination* 199 (1–3) (2006) 501–503, <http://dx.doi.org/10.1016/j.desal.2006.03.193>.
- [46] J.-C. Remigy, M. Meireles, X. Thibault, Morphological characterization of a polymeric microfiltration membrane by synchrotron radiation computed microtomography, *J. Membr. Sci.* 305 (1–2) (2007) 27–35, <http://dx.doi.org/10.1016/j.memsci.2007.06.059>.
- [47] K. Park, J.H. Kim, B.J. Kim, S.J. Cho, J. Hong, G. Lim, Direct visualization of microscale dynamics of water droplets on under-oil-hydrophilic membranes by using synchrotron white-beam X-ray microimaging techniques, *Langmuir : ACS J. Surf. Colloids* 36 (35) (2020) 10548–10554, <http://dx.doi.org/10.1021/acs.langmuir.0c01867>.
- [48] K. Park, D. Lee, J.-H. Lim, J. Hong, G. Lim, Four-dimensional visualization of microscale dynamics of membrane oil fouling via synchrotron radiation microcomputed tomography, *Langmuir : ACS J. Surf. Colloids* (2022) <http://dx.doi.org/10.1021/acs.langmuir.2c01051>.
- [49] S.J. Normile, D.C. Sabarirajan, O. Calzada, V. de Andrade, X. Xiao, P. Mandal, D.Y. Parkinson, A. Serov, P. Atanassov, I.V. Zenyuk, Direct observations of liquid water formation at nano- and micro-scale in platinum group metal-free electrodes by operando X-ray computed tomography, *Mater. Today Energy* 9 (2018) 187–197, <http://dx.doi.org/10.1016/j.mtener.2018.05.011>.
- [50] D. Gabor, A new microscopic principle, *Nature* 161 (4098) (1948) 777, <http://dx.doi.org/10.1038/161777a0>.
- [51] S.C. Mayo, P.R. Miller, S.W. Wilkins, T.J. Davis, D. Gao, T.E. Gureyev, D. Paganin, D.J. Parry, a. Pogany, a.W. Stevenson, Quantitative X-ray projection microscopy: Phase-contrast and multi-spectral imaging, *J. Microscopy* 207 (Part 2) (2002) 79–96, <http://dx.doi.org/10.1046/j.1365-2818.2002.01046.x>.
- [52] R. Hettel, DLSR design and plans: An international overview, *J. Synchrotron Radiat.* 21 (5) (2014) 843–855, <http://dx.doi.org/10.1107/S1600577514011515>.
- [53] A. Björling, S. Kalbfleisch, M. Kahnt, S. Sala, K. Parfeniukas, U. Vogt, G. Carbone, U. Johansson, Ptychographic characterization of a coherent nanofocused X-ray beam, *Opt. Express* 28 (4) (2020) 5069–5076, <http://dx.doi.org/10.1364/oe.386068>.
- [54] S. Kalbfleisch, Y. Zhang, M. Kahnt, K. Buakor, M. Langer, T. Dreier, H. Dierks, P. Stjärneblad, E. Larsson, K. Gordeyeva, L. Chayanun, D. Söderberg, J. Wallentin, M. Bech, P. Villanueva-Perez, X-ray in-line holography and holotomography at the NanoMAX beamline, *J. Synchrotron Radiat.* 29 (Pt 1) (2022) 224–229, <http://dx.doi.org/10.1107/S1600577521012200>.
- [55] J. Soltau, M. Vassholz, M. Osterhoff, T. Salditt, In-line holography with hard x-rays at sub-15 nm resolution, *Optica* 8 (6) (2021) 818, <http://dx.doi.org/10.1364/OPTICA.420060>.
- [56] J. Cesar da Silva, A. Pacureanu, Y. Yang, S. Bohic, C. Morawe, R. Barrett, P. Cloetens, Efficient concentration of high-energy X-rays for diffraction-limited imaging resolution, *Optica* 4 (5) (2017) 492, <http://dx.doi.org/10.1364/OPTICA.4.000492>, URL <https://www.osapublishing.org/abstract.cfm?URI=optica-4-5-492>.
- [57] U. Johansson, D. Carbone, S. Kalbfleisch, A. Björling, M. Kahnt, S. Sala, T. Stankevicius, M. Liebi, A. Rodriguez Fernandez, B. Bring, D. Paterson, K. Thänel, P. Bell, D. Erb, C. Weninger, Z. Matej, L. Roslund, K. Å hnerberg, B. Norsk Jensen, H. Tarawneh, A. Mikkelsen, U. Vogt, NanoMAX: The hard X-ray nanoprobe beamline at the MAX IV Laboratory, *J. Synchrotron Radiat.* 28 (6) (2021) 28, <http://dx.doi.org/10.1107/S1600577521008213>, URL <https://scripts.iucr.org/cgi-bin/paper?S1600577521008213>.
- [58] B. Shi, Y. Fu, Y. Yang, Applications of X-ray holography, *Int. J. Opt.* 2021 (2021) 1–14, <http://dx.doi.org/10.1155/2021/7711028>.
- [59] P.J. Withers, X-ray nanotomography, *Mater. Today* 10 (12) (2007) 26–34, [http://dx.doi.org/10.1016/S1369-7021\(07\)70305-X](http://dx.doi.org/10.1016/S1369-7021(07)70305-X).
- [60] S.-H. Lee, W.-S. Chang, S.-M. Han, D.-H. Kim, J.-K. Kim, Synchrotron X-ray nanotomography and three-dimensional nanoscale imaging analysis of pore structure-function in nanoporous polymeric membranes, *J. Membr. Sci.* 535 (2017) 28–34, <http://dx.doi.org/10.1016/j.memsci.2017.04.024>.

- [61] F. Pfeiffer, X-ray ptychography, *Nat. Photonics* 12 (1) (2018) 9–17, <http://dx.doi.org/10.1038/s41566-017-0072-5>.
- [62] M. Guizar-Sicairos, P. Thibault, Ptychography: A solution to the phase problem, *Phys. Today* 74 (9) (2021) 42–48, <http://dx.doi.org/10.1063/PT.3.4835>.
- [63] M. Dierolf, A. Menzel, P. Thibault, P. Schneider, C.M. Kewish, R. Wepf, O. Bunk, F. Pfeiffer, Ptychographic X-ray computed tomography at the nanoscale, *Nature* 467 (7314) (2010) 436–439, <http://dx.doi.org/10.1038/nature09419>.
- [64] M. Holler, M. Guizar-Sicairos, E.H.R. Tsai, R. Dinapoli, E. Müller, O. Bunk, J. Raabe, G. Aeppli, High-resolution non-destructive three-dimensional imaging of integrated circuits, *Nature* 543 (7645) (2017) 402–406, <http://dx.doi.org/10.1038/nature21698>.
- [65] A. Diaz, P. Trtik, M. Guizar-Sicairos, A. Menzel, P. Thibault, O. Bunk, Quantitative X-ray phase nanotomography, *Phys. Rev. B* 85 (2) (2012) <http://dx.doi.org/10.1103/PhysRevB.85.020104>.
- [66] K. Cramer, N.I. Prasianakis, B. Niceno, J. Ihli, M. Holler, S. Leyer, Three-dimensional membrane imaging with X-ray ptychography: Determination of membrane transport properties for membrane distillation, *Transp. Porous Media* 138 (2) (2021) 265–284, <http://dx.doi.org/10.1007/s11242-021-01603-4>.
- [67] W. Yashiro, C. Kamezawa, D. Noda, K. Kajiwara, Millisecond-order X-ray phase tomography with a fringe-scanning method, *Appl. Phys. Express* 11 (12) (2018) 122501, <http://dx.doi.org/10.7567/APEX.11.122501>.
- [68] F. Schott, B. Dollet, S. Santucci, C. Claudet, M. Argentin, C. Raufaste, R. Mokso, Three-dimensional liquid foam flow through a hopper resolved by fast X-ray microtomography, *Soft Matter* 19 (7) (2023) 1300–1311, <http://dx.doi.org/10.1039/d2sm01299e>.
- [69] A. Khimchenko, C. Bikis, A. Pacureanu, S.E. Hieber, P. Thalmann, H. Deyhle, G. Schweighauser, J. Hench, S. Frank, M. Müller-Gerbl, G. Schulz, P. Cloetens, B. Müller, Hard X-Ray nanoholotomography: Large-scale, label-free, 3D neuroimaging beyond optical limit, *Adv. Sci. (Weinheim, Baden-Württemberg, Germany)* 5 (6) (2018) 1700694, <http://dx.doi.org/10.1002/advs.201700694>.
- [70] V. de Andrade, V. Nikitin, M. Wojcik, A. Deriy, S. Bean, D. Shu, T. Mooney, K. Peterson, P. Kc, K. Li, S. Ali, K. Fezzaa, D. Gürsoy, C. Arico, S. Ouendi, D. Troadec, P. Simon, F. de Carlo, C. Lethien, Fast X-ray nanotomography with sub-10 nm resolution as a powerful imaging tool for nanotechnology and energy storage applications, *Adv. Mater. (Deerfield Beach, Fla.)* 33 (21) (2021) e2008653, <http://dx.doi.org/10.1002/adma.202008653>.
- [71] S. Flenner, M. Storm, A. Kubec, E. Longo, F. Döring, D.M. Pelt, C. David, M. Müller, I. Greving, Pushing the temporal resolution in absorption and Zernike phase contrast nanotomography: Enabling fast in situ experiments, *J. Synchrotron Radiat.* 27 (Pt 5) (2020) 1339–1346, <http://dx.doi.org/10.1107/S1600577520007407>.
- [72] M. Holler, A. Diaz, M. Guizar-Sicairos, P. Karvinen, E. Färm, E. Härkönen, M. Ritala, A. Menzel, J. Raabe, O. Bunk, X-ray ptychographic computed tomography at 16 nm isotropic 3D resolution, *Sci. Rep.* 4 (2014) 3857, <http://dx.doi.org/10.1038/srep03857>.
- [73] M. Guizar-Sicairos, I. Johnson, A. Diaz, M. Holler, P. Karvinen, H.-C. Stadler, R. Dinapoli, O. Bunk, A. Menzel, High-throughput ptychography using Eiger: Scanning X-ray nano-imaging of extended regions, *Opt. Express* 22 (12) (2014) 14859–14870, <http://dx.doi.org/10.1364/OE.22.014859>.
- [74] E. Tudisco, M. Etzegarai, S.A. Hall, E.-M. Charalampidou, G.D. Couples, H. Lewis, A. Tengattini, N. Kardjilov, Fast 4-D Imaging of fluid flow in rock by high-speed neutron tomography, *J. Geophys. Res.: Solid Earth* 124 (4) (2019) 3557–3569, <http://dx.doi.org/10.1029/2018JB016522>.
- [75] H. Dejea, P. Garcia-Canadilla, A.C. Cook, E. Guasch, M. Zamora, F. Crispi, M. Stamparoni, B. Bijnens, A. Bonnin, Comprehensive analysis of animal models of cardiovascular disease using multiscale X-Ray phase contrast tomography, *Sci. Rep.* 9 (1) (2019) 6996, <http://dx.doi.org/10.1038/s41598-019-43407-z>.
- [76] M. Holler, J. Raabe, R. Wepf, S.H. Shahmoradian, A. Diaz, B. Sarafimov, T. Lachat, H. Walther, M. Vitins, OMNY PIN-A versatile sample holder for tomographic measurements at room and cryogenic temperatures, *Rev. Sci. Instrum.* 88 (11) (2017) 113701, <http://dx.doi.org/10.1063/1.4996092>.
- [77] M. Holler, J. Ihli, E. Tsai, F. Nudelman, M. Verezhak, W. van de Berg, S.H. Shahmoradian, A lathe system for micrometre-sized cylindrical sample preparation at room and cryogenic temperatures, *J. Synchrotron Radiat.* 27 (2) (2020) 472–476, <http://dx.doi.org/10.1107/S1600577519017028>.
- [78] J. Schindelin, I. Arganda-Carreras, E. Frise, V. Kaynig, M. Longair, T. Pietzsch, S. Preibisch, C. Rueden, S. Saalfeld, B. Schmid, J.-Y. Tinevez, D.J. White, V. Hartenstein, K. Eliceiri, P. Tomancak, A. Cardona, Fiji: An open-source platform for biological-image analysis, *Nat. Methods* 9 (7) (2012) 676–682, <http://dx.doi.org/10.1038/nmeth.2019>.
- [79] C.D. Hansen (Ed.), *The Visualization Handbook*, [Online-ausg.], Elsevier-Butterworth Heinemann, Amsterdam, 2005.
- [80] Y. Hu, A. Limaye, J. Lu, Three-dimensional segmentation of computed tomography data using Drishti Paint: New tools and developments, *R. Soc. Open Sci.* 7 (12) (2020) 201033, <http://dx.doi.org/10.1098/rsos.201033>.
- [81] S. Berg, D. Kutra, T. Kroeger, C.N. Straehle, B.X. Kausler, C. Haubold, M. Schiegg, J. Ales, T. Beier, M. Rudy, K. Eren, J.I. Cervantes, B. Xu, F. Beuttenmueller, A. Wolny, C. Zhang, U. Koethe, F.A. Hamprecht, A. Kreshuk, Ilastik: Interactive machine learning for (bio)image analysis, *Nat. Methods* 16 (12) (2019) 1226–1232, <http://dx.doi.org/10.1038/s41592-019-0582-9>.
- [82] S. van der Walt, J.L. Schönberger, J. Nunez-Iglesias, F. Boulogne, J.D. Warner, N. Yager, E. Gouillart, T. Yu, scikit-image: Image processing in Python, *PeerJ* 2 (2014) e453, <http://dx.doi.org/10.7717/peerj.453>.
- [83] P. Virtanen, R. Gommers, T.E. Oliphant, M. Haberland, T. Reddy, D. Cournapeau, E. Burovski, P. Peterson, W. Weckesser, J. Bright, S.J. van der Walt, M. Brett, J. Wilson, K.J. Millman, N. Mayorov, A.R.J. Nelson, E. Jones, R. Kern, E. Larson, C.J. Carey, Í. Polat, Y. Feng, E.W. Moore, J. VanderPlas, D. Laxalde, J. Perktold, R. Cimrman, I. Henriksen, E.A. Quintero, C.R. Harris, A.M. Archibald, A.H. Ribeiro, F. Pedregosa, P. van Mulbregt, SciPy 1.0: Fundamental algorithms for scientific computing in Python, *Nat. Methods* 17 (3) (2020) 261–272, <http://dx.doi.org/10.1038/s41592-019-0686-2>.
- [84] J. Gostick, Z. Khan, T. Tranter, M. Kok, M. Agnaou, M. Sadeghi, R. Jervis, PoreSpy: A Python toolkit for quantitative analysis of porous media images, *J. Open Source Software* 4 (37) (2019) 1296, <http://dx.doi.org/10.21105/joss.01296>.
- [85] E. Larsson, D. Gürsoy, F. de Carlo, E. Lilleodden, M. Storm, F. Wilde, K. Hu, M. Müller, I. Greving, Nanoporous gold: A hierarchical and multiscale 3D test pattern for characterizing X-ray nano-tomography systems, *J. Synchrotron Radiat.* 26 (Pt 1) (2019) 194–204, <http://dx.doi.org/10.1107/S1600577518015242>.
- [86] M.D. de Jonge, S. Vogt, Hard X-ray fluorescence tomography—An emerging tool for structural visualization, *Curr. Opin. Struct. Biol.* 20 (5) (2010) 606–614, <http://dx.doi.org/10.1016/j.sbi.2010.09.002>.
- [87] M. Kahnt, G. Falkenberg, J. Garrevoet, J. Hartmann, T. Krause, M. Niehle, M. Scholz, M. Seyrich, A. Trampert, A. Waag, H.-H. Wehmann, F. Wittwer, H. Zhou, M. Hanke, C.G. Schroer, Simultaneous hard X-ray ptychographic tomography and X-ray fluorescence tomography of isolated hollow core-shell GaN Rods, *Microsc. Microanal.* 24 (S2) (2018) 34–35, <http://dx.doi.org/10.1017/S143192761801259X>.